AD-A111 453 NAVAL RESEARCH LAB WASHINGTON DC F/G 10/3
RESEARCH ON LEAD ACID BATTERY ELECTRODES.(U)
FEB 82 A C SIMON, S M CAULDER, C P WALES EC-76-A-31-1003
UNCLASSIFIED NRL-MR-4751 NL

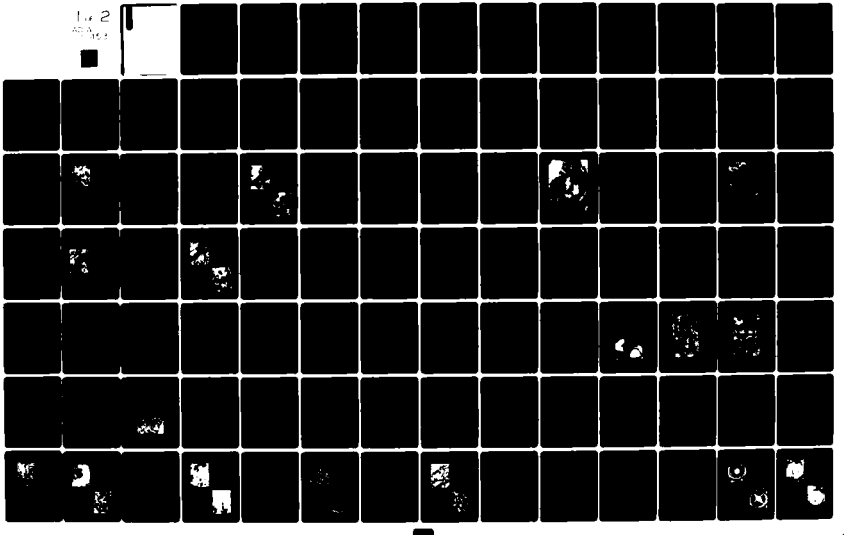

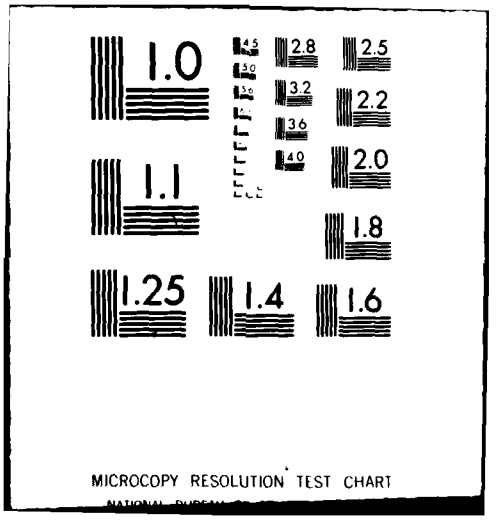
1.0
1.1
1.25
1.4
1.6
1.8
2.0
2.2
2.5
2.8
3.2
3.6
4.0
4.5
5.0
MICROCOPY RESOLUTION TEST CHART

SECURITY CLASSIFICATION OF THIS PAGE (When Data Entered)

REPORT DOCUMENTATION PAGE		READ INSTRUCTIONS BEFORE COMPLETING FORM
1. REPORT NUMBER NRL Memorandum Report 4751	2. GOVT ACCESSION NO. AD-A114	3. RECIPIENT'S CATALOG NUMBER 453
4. TITLE (and Subtitle) RESEARCH ON LEAD ACID BATTERY ELECTRODES		5. TYPE OF REPORT & PERIOD COVERED A final report on the problem. 6. PERFORMING ORG. REPORT NUMBER
7. AUTHOR(s) A.C. Simon, S.M. Caulder, C.P. Wales and R.L. Jones		8. CONTRACT OR GRANT NUMBER(s)
9. PERFORMING ORGANIZATION NAME AND ADDRESS Naval Research Laboratory Washington, DC 20375		10. PROGRAM ELEMENT, PROJECT, TASK AREA & WORK UNIT NUMBERS 61-0026-01
11. CONTROLLING OFFICE NAME AND ADDRESS U.S. Department of Energy Washington, DC 20545		12. REPORT DATE February 26, 1982 13. NUMBER OF PAGES 104
14. MONITORING AGENCY NAME & ADDRESS(if different from Controlling Office)		15. SECURITY CLASS. (of this report) UNCLASSIFIED 15a. DECLASSIFICATION/DOWNGRADING SCHEDULE

16. DISTRIBUTION STATEMENT (of this Report)

Approved for public release; distribution unlimited.

17. DISTRIBUTION STATEMENT (of the abstract entered in Block 20, if different from Report)

18. SUPPLEMENTARY NOTES

For the U.S. Department of Energy, Energy Storage Systems Division under Interagency Agreement No. EC-76-A-31-1003 (DE-AP-03-80-SF-11185)

19. KEY WORDS (Continue on reverse side if necessary and identify by block number)

Batteries
Energy storage
Kinetics of electrode processes

20. ABSTRACT (Continue on reverse side if necessary and identify by block number)

The reactions and physical and molecular transformations that occur in lead acid battery plate active material during charge-discharge cycling have been studied under a DOE program to improve the lead acid battery for electric vehicle applications. Investigations included structural studies of PbO_2 by x-ray/neutron diffraction, effects of cycling on capacity by pulsed vs unpulsed discharge, active material microstructure/plate capacity changes under high EV-type discharge rates, "coralloid" structure formation in cycled positive plates, and tubular plate active material changes during formation and cycling.

DD FORM 1 JAN 73 1473 EDITION OF 1 NOV 65 IS OBSOLETE
S/N 0102-014-6601

SECURITY CLASSIFICATION OF THIS PAGE (When Data Entered)

CONTENTS

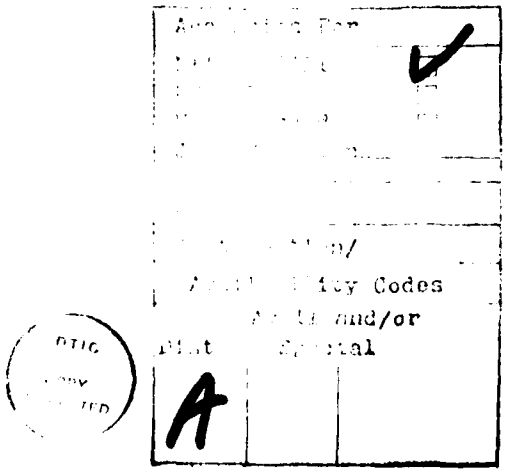

Extended Abstract

For successful electric vehicle application, lead acid batteries require improved energy density and extended deep-discharge cycle life. Improved energy density can come from increased utilization of the plate (electrode) active material, which even in the latest batteries seldom exceeds 35-40%. Cycle life is also principally determined by the plate active material, i.e., by the reactions and physical changes that occur in the active material with cycling and cause it to lose capacity to accept charge. Rational approaches to significantly improving lead acid battery performance must rely heavily therefore on understanding the reactions of the plate active material.

This report describes several investigations which elucidate important reactions or transformations occurring in plate active material that are relevant to electric vehicle operation.

Formation of electrochemically inactive PbO_2(i.e., a form of PbO_2 not reduced in plate discharge) is a substantial cause of positive plate capacity loss. Electrochemically active PbO_2 contains a proton species lacking in the inactive form, as revealed by NMR results at NRL, and a neutron/x-ray diffraction structure determination was undertaken to establish the proton lattice location. This has proven difficult, and while the first two steps, i.e., the high resolution structure determinations of chemically prepared (inactive, non-proton bearing) β-PbO_2 and α-PbO_2 were essentially completed (the α-PbO_2 data is in process of interpretation and the structure is expected to be published), the third step, comparison with the structure of electrochemically produced (and active) PbO_2, could not be completed in the contract period. The two "base line" structures, and the computational and experimental procedures, have been established however, and future research, at NRL or elsewhere, may build on these results.

In a second major effort, the potential effects of high discharge rates in electric vehicles were investigated by comparing changes in the active material microstructure and plate capacity for positive and negative lead-acid plates cycled at discharge rates ranging from 18 to 2000 A/m^2. Comparisons were also made between pulsed (used in electric vehicles) and unpulsed discharge modes. The negative plate capacity decreased significantly with discharge rate, being ~2X less for 2000 A/m^2 than 18 A/m^2 rates. Capacity decreased also with cycling, apparently because of development of reduced contact between the lead particles in the charged plate and/or formation of $PbSO_4$ passivating layers on the Pb particles during discharge, especially at high rates. The positive plate capacity was strongly affected by discharge rate, decreasing by 4X in going from 18 A/m^2 to 2000 A/m^2 rates. Capacity losses with cycling were greater than with negative plates, and appeared to result largely from progressive formation of electrochemically inactive PbO_2 during cycling. Pulsed discharge was detrimental to plate capacity, but less for the negative plate than the positive plate. Careful analysis was made of the active material particle size, surface area, composition, and porosity to help explain plate performance under the different discharge rates.

The positive plate active material has been shown in this laboratory, both with test plates and in-service batteries, to develop a characteristic coral-like, or coralloid, structure with cycling. This structure is densely packed, and PbO_2 in its interior is difficult to reduce on discharge, resulting in capacity loss. Limited experiments were undertaken in the present work to determine if coralloid formation could be prevented, or its dimensions reduced, by different methods or materials of plate preparation. Procedures were found which delayed coralloid formation, e.g., using tetrabasic lead sulfate as the initial plate material, but in each case, the coralloid ultimately formed as cycling continued.

The performance and microstructure of tubular battery plates were also studied, since this construction, although little used

in the U.S., offers long cycle life as required for electric vehicle use. Results from this research indicate that prolonged preliminary soaking of tubular plates, as normally practiced by manufacturers, may be unnecessary. Also bursting of tubes, a major cause of tubular plate failure, was shown to be primarily caused by corrosion of the current-collecting lead spline, with formation of corrosion products of higher volume than the original metal, and not by the normal volume change in active material that accompanies plate formation or cycling.

RESEARCH ON LEAD ACID BATTERY ELECTRODES
Final Report

I. INTRODUCTION

A. BACKGROUND

The lead-acid battery is an electrochemical device in which the chemical energy from oxidation-reduction reactions is made available in the form of electrical energy. Although this battery is one of the oldest sources of electric power, the understanding of the mechanisms and reactions involved is a comparatively recent development. The lead-acid battery has been developed largely on an empirical basis, with primary concern on economics of manufacture and performance in light, intermittent application such as automotive starting-lighting-ignition. To develop lead-acid batteries giving long and efficient life under deep-discharge cycling usage such as in electric vehicles or power generation load leveling will require a new level of understanding of lead-acid battery reactions.

The performance of the lead-acid battery depends on many factors, some of which might be called mechanistic and others that might be considered as resulting from engineering and design. The mechanistic factors determine the ease with which the electron is transferred from its normal or rest state and made to do useful work. This involves the electrochemical and thermodynamic principles that determine the energy obtained from the charge transfer reaction and the transport of the

Manuscript submitted December 29, 1981.

reactive species from the electrode surface.

The Pb/H_2SO_4 electrode has been studied in considerable detail using x-ray, calorimetric, thermogravimetric and differential thermal analysis, and cyclic voltammetry, chronopotentiometry and other electroanalytical methods. Thus, the chemical reactions, thermodynamics and the limiting conditions for the release of energy at the molecular level, and the charge-transfer mechanism and the transport to and from the electrode are fairly well understood. In addition, the engineering design of battery electrodes, separators, cases and other cell components has progressed markedly in recent years.

It must be recognized, however, that the electrochemistry of lead-acid battery electrodes, or plates, is much more complex than that of simple, non-porous, pure lead-acid electrodes which have been studied classically. The electrodes of the working battery are composed of a porous mass of considerable depth and complexity, which has a large and variable capacity influenced by factors such as: surface area; the size and tortuosity of pore development; the reproducibility of the crystal structure; the electrolyte concentration within the pores; the generation or retention of gas bubbles; the size and habit of the lead, lead sulfate, and lead dioxide crystals that are involved in reaction. Other problems also arise in maintaining the conductivity of the reactive materials, collecting current from the active mass, maintaining cohesion between the particles of the active mass and keeping the mass within the grid.

Scale-up from the simple sheet electrodes used in mechanistic studies introduces still more problems, e.g., unequal current distribution in and between electrodes, gravity and pressure effects introduced by the size and weight of the electrode, volume changes within the electrode structure, and stratification of the electrolyte.

Yet it is from improved understanding of this little known and difficult area, the electrode active material and its reactions, that increased capabilities for the lead-acid battery are most likely to come. The lead-acid battery is well known to give low utilization of electrode material, less than 50% under the most favorable conditions and more often near 35%. The cause of failure of the battery, especially under deep-discharge cycling service, also normally lies with the electrode active material, viz; through reactions and changes in the electrode mass that lead to its softening, spalling and refusal to accept charge. Increasing the lead-acid battery's specific energy and deep-discharge cycle life, as required for electric vehicle and load leveling use, is therefore principally and inexorably bound with understanding the reactions, and improving the performance, of the electrode active material.

Considerable progress has in fact been made in the understanding of lead-acid active material reactions. One important cause for loss of charge capacity that we have identified is the formation of an electrochemically inactive type of PbO_2 in the battery positive plate, the amount of which increases progressively with the number of charge-discharge cycles. This inactive

PbO_2, which is not reduced on discharge and makes no contribution to cell capacity, has been shown by NMR analysis to be deficient in a proton species present in electrochemically active PbO_2 (1). We have also identified, from experiments and examination of service batteries, a characteristic coral-like, or coralloid, microstructure that forms in positive plate active material with cycling (2). This coralloid structure appears to form universally, occurring earlier or later depending on the individual battery and cycle regime, but nonetheless always forming, and when formed, apparently largely controlling the positive plate performance. A loss of capacity is normally noted, for example, as the coralloid develops, which we believe is due to the coralloid nodules being dense and of such diameter as to prevent PbO_2 in their interior from being completely reduced during discharge. It would clearly be helpful in improving positive plate performance if we could understand the formation of this fundamental microstructure, and how it may be prevented or the coralloid features modified.

B. OBJECTIVES OF THE INVESTIGATION

The principal objective of the investigation has been therefore to extend the understanding of lead-acid active material reactions by ascertaining how the physical and molecular nature of the active material are affected by repetitious charge and discharge under current rates, pulsed discharge and/or other conditions relevant to electric vehicle application.

In another part of the investigation, battery components and batteries from electric vehicle (EV) service and tests were

examined, and their properties and microstructure compared with those obtained in laboratory experiments. This served to insure the relevance of the laboratory findings, as well as providing guidance and aid in problem solving to DOE program members engaged in EV battery development.

The following sections describe some of the observations and conclusions that have been a product of this investigation.

II. STRUCTURAL STUDIES OF LEAD DIOXIDE

A. BACKGROUND

There are two known polymorphic crystalline forms of lead dioxide. The naturally occurring plattnerite with a rutile-type structure has been designated as β-PbO_2. The other form, designated as α-PbO_2, has not been found under natural conditions. The alpha form of PbO_2 has the orthorhombic crystal form, while the beta form has the tetragonal structure. There are various chemical methods of preparing β-PbO_2, as well as obtaining it from the mineral, but it is also formed when a paste consisting of a mixture of PbO and basic lead sulfates (principally monobasic $PbO \cdot PbSO_4$, and tribasic $3PbO \cdot PbSO_4 \cdot H_2O$) is allowed to harden by drying and is then subjected to electrolysis. This is the so-called "forming process" by which the positive plate of the lead-acid battery is converted to PbO_2. Beta PbO_2 is the oxide predominantly formed when the discharged positive plate, containing mostly $PbSO_4$, is charged and recoverted to PbO_2, although in most cases, the product is a mixture of the alpha and beta forms. Under very acid conditions, the product will be almost entirely β-PbO_2, while in alkaline solutions, α-PbO_2 will be the principal product.

Commercially available β-PbO_2 that is chemically prepared appears to be mostly electrochemically inactive; one reason why the positive plate is not directly pasted with available PbO_2 instead of consuming time and energy to electrolytically form β-PbO_2. There is no commercially available α-PbO_2. The electrochemical form of α-PbO_2 can be obtained by oxidation of PbO in 2N NaOH solution at 20°C, using a current of 1 ma/cm^2. Chemically prepared α-PbO_2 can be synthesized by ammonium persulfate oxidation of lead acetate in a strongly ammoniacal solution of ammonium acetate. Unless extreme precautions are taken, the preparation of either polymorph will be contaminated by the other.

We previously found by nuclear magnetic resonance studies (NMR) that electrochemically active PbO_2 is characterized by the presence of a proton species, probably an OH radical, that somehow fits into the PbO_2 lattice. This proton species was almost completely absent from the chemically prepared PbO_2 (1). We believe therefore that the proton species is somehow essential to electrochemical activity.

The manner in which the proton species contributes to electrochemical activity could conceivably be understood if its position in the lattice were known. The determination of the location of a small number of protons in a metal-oxide lattice is difficult, but it was deemed possible using combined x-ray and neutron diffraction with advanced computation procedures developed in the NRL Structure of Matter group, and the study was undertaken. For this investigation, the crystal structure of chemically prepared (i.e., non-proton containing) β-PbO_2 must be very

accurately known. Review of the literature showed that previous β-PbO_2 structure determinations were not sufficiently accurate and contained discrepancies. The initial task therefore was to make a high resolution re-determination of the structure of chemically prepared β-PbO_2. An accurate determination of the α-PbO_2 structure is also necessary, since, although mainly β-PbO_2, electrochemically formed PbO_2 may contain substantial amounts of α-PbO_2. These two structures will then serve as a "baseline" for comparison with the electrochemically active PbO_2 to give the proton lattice site locations.

B. BRIEF DESCRIPTION OF EXPERIMENTAL METHOD

The neutron diffraction data were collected at the National Bureau of Standards. This high resolution neutron reactor facility uses a multiple channel detector which reduces data collecting time by a factor of 4. Data were collected up to sin θ/λ of 0.6 in five overlapping ranges: 15.0-40.0, 35.0-60.0, 55.0-80.0, 75.0-100.0 and 95.0-120.0° at intervals of 0.05°.

The five overlapping ranges of data were treated for systematic errors and scaled. Refinement of the structure of PbO_2 was accomplished using the Rietveld method (3). This method does not employ neutron powder intensities, but directly uses the profile intensities that are obtained from the step-scanning measurements. This procedure was modified so as to simultaneously process the data from the five channels of the multiple channel detector.

C. RESULTS AND DISCUSSION

Chemically prepared β-PbO_2 is tetragonal with two molecules per unit cell and the atoms are in the following special positions of the space group D_{4h}^{14} (P_4/mnm):

Pb (2a) ooo; 1/2,1/2,1/2

O (4f) ± (uuo; u + 1/2, 1/2-u, 1/2)

The unit cell parameters and the oxygen positional parameter, u, are compared with earlier work in Table I. The cell volume is 83.27 A^3 (4).

Tolkacev (5) used x-ray diffraction to study the structure of PbO_2. He did not quote any errors on his cell parameters and oxygen positional parameter. His cell constants were found to be about 0.25% low and u 0.4% high compared with our work. Leciejewicz and Padlo (6) have used neutron diffraction to study the structure of tetragonal β-PbO_2. The unit cell parameters, a and c, determined by these investigators were found to be 0.05% and 0.14% low compared to our work, respectively, and u is 0.75% larger than in the present investigation.

The data obtained extended to sin θ/λ = 0.6. The resolution of the profile enabled the background to be evaluated at selected positions at low and high angle, permitting an anisotropic thermal refinement. Up to the present, there has been no thermal parameter treatment reported for PbO_2. Since the atoms are situated on special positions of the space group D_{4h}^{14}, the components of the thermal motion ellipsoid are restricted according to the point symmetry of the site. The symmetry of lead is

Table I
Comparison of Tetragonal Unit Cell and Positional
Parameters of Chemically Prepared β-PbO_2 With Earlier Results

Source	Method	a, Å	c, Å	u
This work (26)	ND-P	4.9578(2)	3.3878(2)	0.3067(2)
	ND-I	4.9576(2)	3.3881(3)	0.3067(8)
Tolkachev	XD	4.946	3.379	0.308
Leciejewicz and Padlo	ND	4.955(3)	3.383(2)	0.309(4)

ND-P - Neutron Diffraction Profile

ND-I - Neutron Diffraction Intensity

XD - X-ray Diffraction

Numbers in parentheses are uncertain

mmm and for oxygen it is mm. The thermal ellipsoid components for both atoms, which are listed in Table II, are restricted such that $\beta_{11}=\beta_{22}$ and $\beta_{13}=\beta_{23}=0$. Thermal parameters of the form exp $(-\beta_{11}h^2-\beta_{33}l^2-2hk\beta_{12}-2hl\beta_{13}-2hl\beta_{23})$ were used.

The derived structure of chemically prepared β-PbO_2 is shown in Fig. 1. The atoms are represented by their thermal ellipsoids. The major vibrational motion of the oxygen atoms is perpendicular to the equatorial octahedral planes. The six oxygen atoms surrounding each lead atom do not form regular octahedra since the four Pb-O distances in the equatorial plane are longer than the two axial Pb-O distances. In Fig. 2 the oxygen atoms are connected to demonstrate the octahedral packing sequence. The structure is composed of vertical columns along [001] of PbO_6 octahedra. The columns repeat along a and b by a unit cell translation. These columns are joined together by another array of octahedral columns oriented at 90° to the first group with the line joining their apices parallel to [110]. This arrangement results in equatorial oxygens of one group becoming axial oxygens of the other group.

In Table III the principal interatomic distances and angles in a PbO_6 octahedral coordinate sphere are compared with the results of Leciejewicz et al (6). The atom designations refer to Fig. 3. These authors appear to have incorrectly calculated the O(1)....O(3,4,5,6) and O(2)....O(3,4,5,6) distances, as well as the O-Pb-O angles. The O-Pb-O angles were also misassigned. For comparison purposes, their oxygen position parameter, cell dimensions, and error estimate were used to

Table II
Comparison of Anisotropic Thermal Parameters Determined by the Rietveld (3) Method and ORFLS (7) Refinement on Integrated Intensities

Atom	$\beta_{11}=\beta_{22}$	β_{33}	β_{12}	$\beta_{13}=\beta_{23}$
Lead				
ND-P	0.0055(4)	0.005(1)	0.0003(6)	0
ND-I	0.0067(22)	0.006(6)	0.0001(40)	0
Oxygen				
ND-P	0.0097(5)	0.008(2)	-0.0055(7)	0
ND-I	0.0081(28)	0.022(7)	-0.004(4)	0

Numbers in parentheses are uncertain.

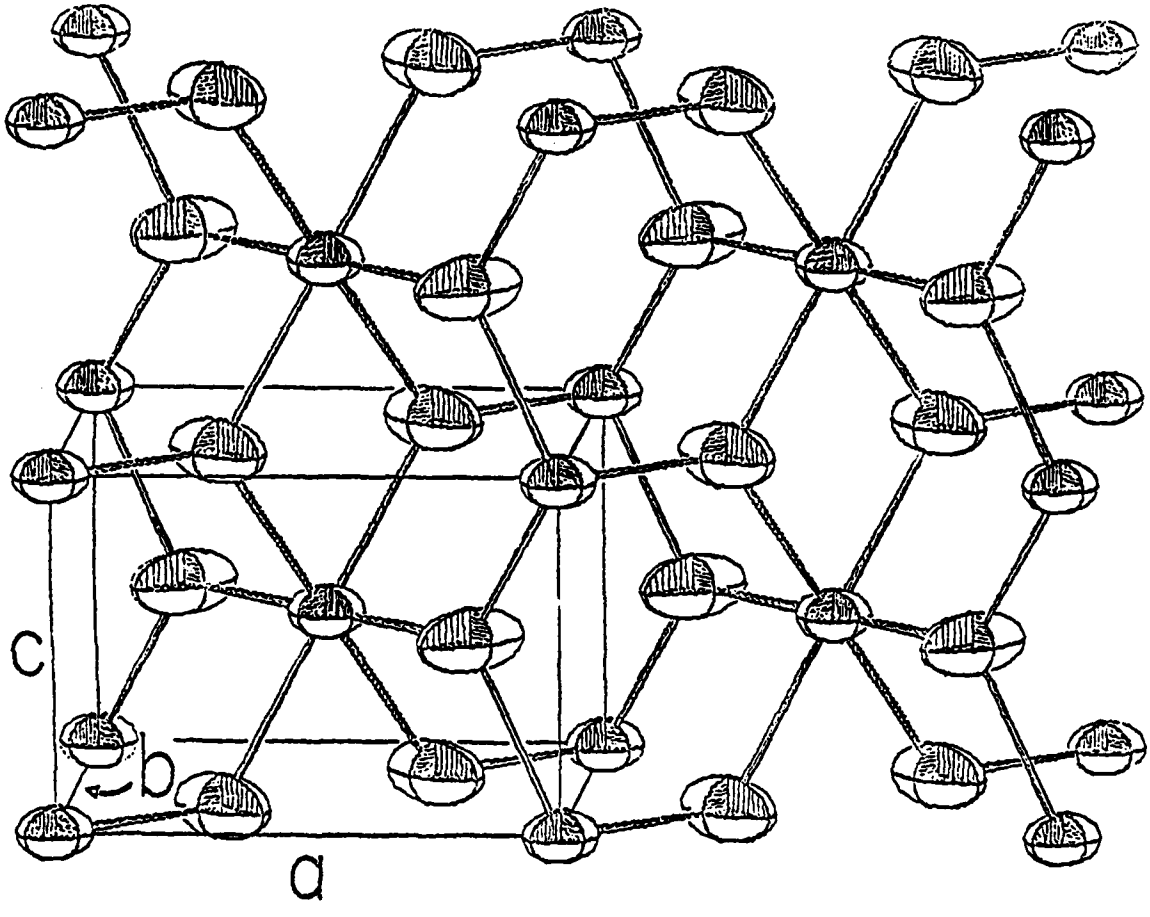

Fig. 1 — Packing diagram for chemically prepared βPbO_2, showing thermal ellipsoids and unit cell outline. Principal oxygen displacement is seen to be perpendicular to the octahedral equatorial plane.

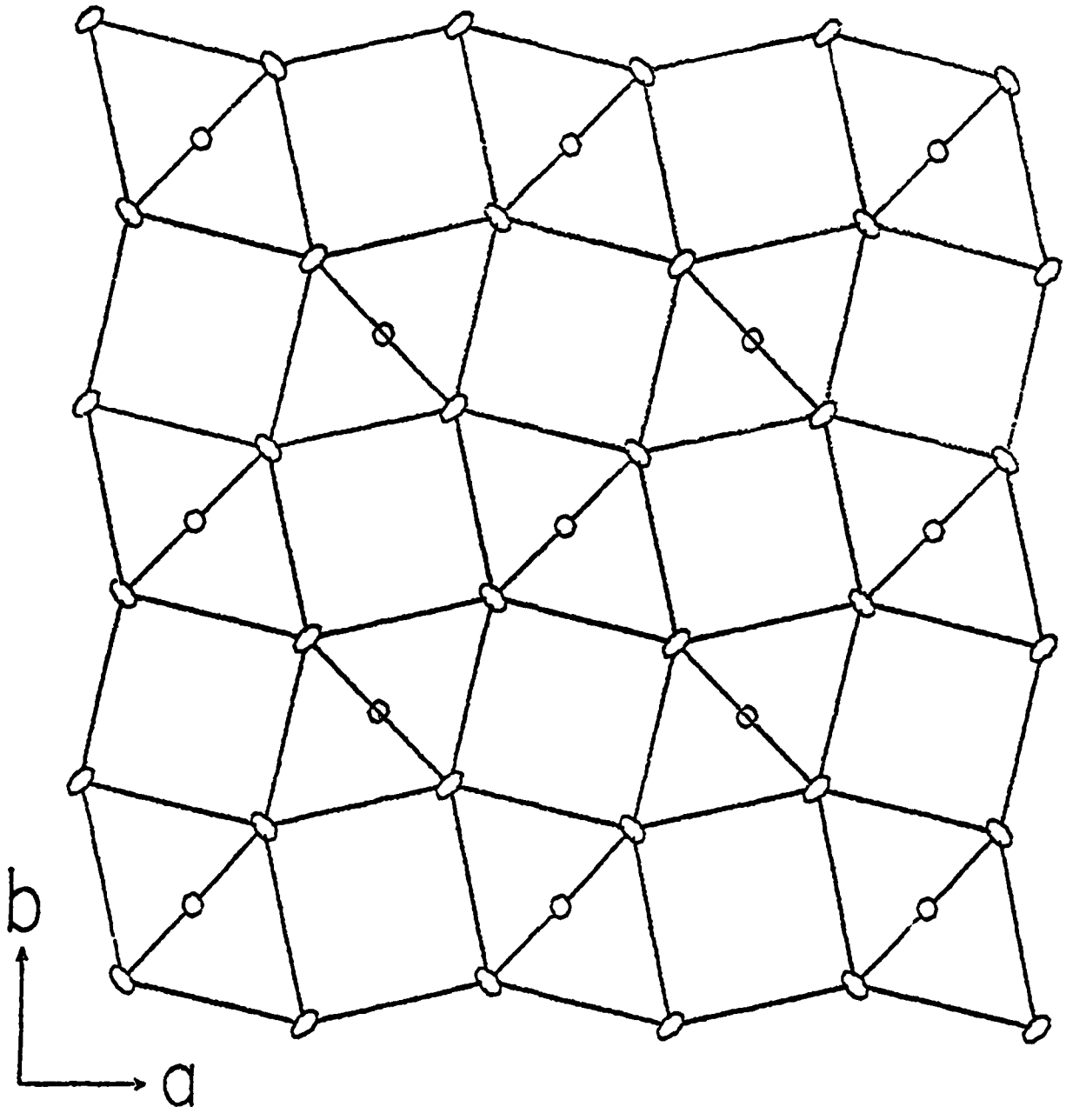

Fig. 2 — Projection of the structure of chemically prepared β-PbO_2 down the c axis. The oxygen atoms are connected to illustrate the octahedral packing scheme. Two types of octahedral columns parallel to the [001] direction are oriented 90° with respect to each other and are joined apex to equatorial atom.

Table III
Comparison of Principal Distances and Angles in the Octahedral Coordination Sphere of Chemically Prepared β-PbO_2 with Earlier Results

	This Work (26)		Liejewicz and Padlo	
	Distance(Å)	Angle(°)	Distance(Å)	Angle(°)
Pb-O(1,2)	2.1502(11)		2.165(20)	
Pb-O(3,4,5,6)	2.1695(7)		2.157(12)	
O(3)...O(4) O(5)...O(6)	2.71110(22)		2.677(40)	
O(1)...O(3,4,5,6) O(2)...O(3,4,5,6)	3.0545(4)		3.056(8)	
O(3)...O(6) O(4)...O(5)	3.3878(2)		3.383(2)	
O(1)-Pb-O(2)	4.3004(22)	180.00(0)	4.331(4)	180.00
O(1)-Pb-O(3,4,5,6) O(2)-Pb-O(3,4,5,6)	3.0545(4)	90.00(1)	3.056(8)	90.0(2)
O(3)-Pb-O(6) O(4)-Pb-O(5)	3.3878(2)	102.66(5)	3.383(2)	103.3(8)
O(3)-Pb-O(4) O-5)-Pb-O(6)	2.7110(22)	77.34(5)	2.677(40)	76.7(8)

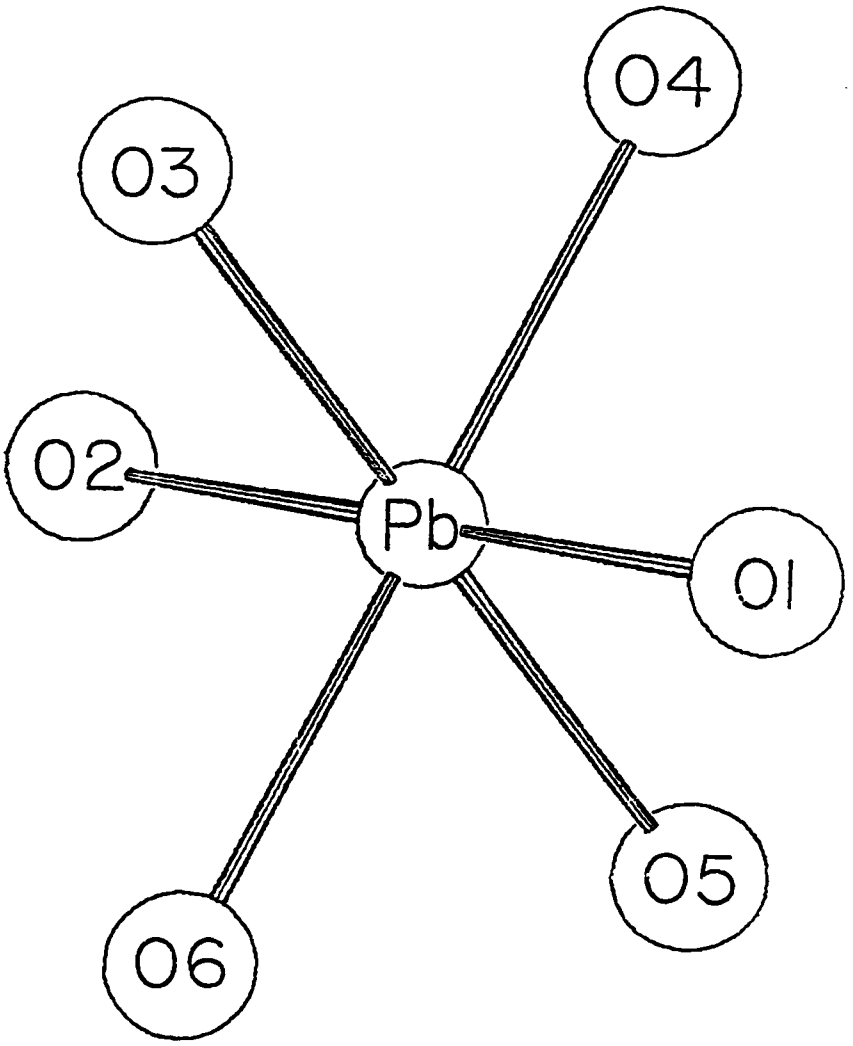

Fig. 3 — Orientation and assignment of the six octahedrally coordinated oxygens around lead in chemically prepared β-PbO_2. The octahedral is irregular with the four Pb-O(3,4,5,6) distances larger than the two Pb-O(1,2) distances.

recalculate the non-bond distances and angles in question with their associated errors. These latter recalculated values are included in Table III.

Since the oxygen positional parameter was 0.002A larger than the value obtained in the present determination, the reported Pb-O distances in the equatorial octahedral plane were smaller than the axial distances. This was just the opposite of what was found in the present determination. In addition, their larger positional parameter caused the O(3)-Pb-O(4) angle to be smaller than in the present case and the O(3)-Pb-O(6) angle to be larger.

The structure and anisotropic thermal parameters of chemically prepared β-PbO_2 have been determined with high accuracy and attention called to some errors and differences with earlier studies. A similar determination undertaken for chemically prepared α-PbO_2 was slowed by difficulties in preparing beta-free α-PbO_2, and instrumental problems at the neutron diffraction facility. However, the experimental portion of the α-PbO_2 investigation has been completed, with the data currently in the process of interpretation. The α-PbO_2 structure is expected to be published later, with appropriate acknowledgement of DOE support, even though the present contract is closed.

III. EFFECTS OF CYCLING REGIME ON CAPACITY

A. BACKGROUND

Electric vehicles (EV) require battery discharges over a range of current densities that may extend to very high values. The type of service that is expected for batteries in EVs varies

considerably from that usually demanded of batteries. Consequently, it is important to determine what effect discharges at different rates may have on the microstructure of lead-acid electrodes and to find how such structural changes affect the capacity and life of a battery.

Repeated cycles of charge-discharge cause a gradual loss of capacity and life, with capacity being additionally reduced as the rate of discharge increases. This latter loss of capacity is attributed to the inability of the electrolyte to diffuse rapidly enough into the plate, so that active material within the plate reacts progressively less with increasing rates of discharge.

However, there are crystal growth processes which must also occur in charge and discharge. For the positive plate active material, the overall reaction is

$$PbO_2 + 4\ H^+ + SO_4^{--} + 2\ e^- \rightleftharpoons PbSO_4 + H_2O$$

and one has crystals of lead dioxide being dissolved, and crystals of lead sulfate being formed in discharge, with the reverse occurring during charge. For the negative plate, the reaction is

$$Pb + SO_4^{--} \rightleftharpoons PbSO_4 + 2\ e^-$$

with lead dissolved and lead sulfate formed in discharge, and the reverse in charge. These growth/dissolution processes are drastically affected by the discharge (charge) rate, with the crystals produced showing substantial differences in factors (size, surface area, porosity, conductivity) which affect the electrode's reactivity and capacity. Very little quantitative

knowledge is available in this area, especially for very high discharge rates, and systematic investigations of the type undertaken here are strongly needed.

From many studies of crystal growth, it has been established that slow rates of growth favor the formation of a relatively few crystals and that these grow to large size with a regular growth habit. Rapid rates of growth produce much more nucleation of crystals that grow to smaller size and with less regular growth habit. In many cases very high rates of growth produce crystals that have only a dendritic skeleton to outline the preferred planes of growth. In addition, in the case of the lead-acid battery, the lead sulfate formed during discharge is very insoluble, and $PbSO_4$ crystals may form on the lead or lead oxide crystals from which the lead ions originate producing passivating" layers of $PbSO_4$ that greatly reduce further reaction.

Thus, the rate of electrode reaction may be influenced by factors other than electrolyte diffusion. A battery being used in an electric vehicle undergoes brief pulses of very high discharge when accelerating or hill climbing, followed by intervals of discharge at much lower rate, which is unlike the discharge-charge regimes required in most battery service.

Cruise driving requires a considerable rate of battery discharge and undoubtedly concentration gradients are set up in the electrolyte in the pores extending from the surface to the interior of the active material. Under normal driving conditions, sufficient ions are presumably transported through the pores to allow the electrode reaction to proceed even at the plate

interior. But a sudden pulse of high current demand will cause most of the reaction to take place at or near the surface, so that no ions proceed along the electrolyte gradient to the deep interior. Not only does the increased growth of lead sulfate near the surface tend to block the pores, but it is possible, if the pulses occur sufficiently close together, that there will be insufficient time to re-establish the original gradient. Since the ions being removed are $SO_4^{=}$, and the acid electrolyte is being converted by water, the specific gravity may be reduced sufficiently so that lead sulfate may begin to dissolve at the plate interior. Thus it is of interest, and of potential benefit in understanding electrode reactions, to determine how pulsed discharges, repeated over a period of time, will affect the structure of the active material.

B. PULSED VERSUS UNPULSED DISCHARGE

In a preliminary experiment, two batteries were connected in series (six cells) and discharged at 145 amperes d.c. for 142 cycles. The ratio of watt hours compared to those achieved in a National Electrical Manufacturers Association (NEMA) standard 75 ampere discharge ranged from 0.89 to 0.94 with a peak of 0.94 from cycles 55 to 85.

These results were compared with those from two similar batteries that were pulse-discharged at 167 Hertz with 290 ampere peaks and a 50% duty cycle, i.e., at the same average 145 ampere rate, with rise and fall times of 0.2 millisecond. The ratio of watt-hours to a NEMA 75 ampere discharge ranged from 0.75 to 0.84 with peaks of 0.83 to 0.85 at cycles 25 through 65. An

unpulsed discharge at 145 amperes was performed at cycle 37 with a NEMA ratio of 0.80. This suggests that a battery may become conditioned by pulsed discharge and yield less capacity when an unpulsed discharge follows.

Examination of the active material structure by microscopy showed several differences between the pulsed and unpulsed batteries. In the pulsed positive plate, the coralloid structure had smaller pores (Fig. 4) in the charged state and the interconnection of aggregates of particles was more evident than in the unpulsed battery (Fig. 5). In addition, the central portions of the aggregates appeared to be nonporous, whereas in the unpulsed plate, the aggregates appeared loosely grouped and porous. Also, at the center of the pulse-discharged positive plate, there were numerous large lead sulfate crystals, even though the plate had been removed in the charged state. This is very unusual and would be a factor tending to reduce plate capacity. Also, the lead dioxide surrounding these lead sulfate crystals had particles that were unusually small.

X-ray diffraction analysis of the charged positive plate from the unpulsed battery showed a high content of β-PbO_2 and a minor amount of α-PbO_2, whereas the pulsed positive plate in the charged state showed β-PbO_2 but with a larger amount of α-PbO_2, as well as considerable $PbSO_4$.

These results left little doubt that high rate pulses affected the positive active material. Physical changes were also noted in the negative plate after pulsing. Whereas the changes in the positive plate appeared to be detrimental to capacity, those in

Fig. 4 — Metallurgical cross-section of vacuum impregnated positive plate active material. Dark areas are former pores, now filled with plastic. Light areas are PbO_2. This plate was cycled using pulsed discharges. Note the dense appearance of the PbO_2 areas and the fact that they seem to be interconnected. Optical microscope photograph, vertical illumination, reflected light. Magnification 1000X.

Fig. 5 — Compare with Fig. 4. Conditions are similar except the plate here was not pulse discharged during cycling. Note that PbO_2 areas are more porous and less interconnected and that pore areas are also larger. Magnification 1000X.

the negative plate appeared to be beneficial. Since the batteries had undergone a large number of cycles before examination, it was not known whether these effects were produced repeatedly during each discharge cycle or were the cumulative effect of all of the previous cycling.

To determine whether the effect was cumulative and to observe the magnitude of the microstructural changes produced by discharges at different current densities, the discharge rate effects were studied individually on the positive and negative electrodes. When studying the effects at either electrode, a much larger counter electrode was employed, as well as an excess of electrolyte. This was to make certain that the electrode under investigation was actually limiting the reactions.

C. DISCHARGE RATE EFFECTS ON THE NEGATIVE PLATE

1. Background

While the microstructure of the negative plate of the lead-acid battery has been studied to some extent by other investigators (8-12), there has been little or no effort to correlate the results of such investigations with either discharge rates or capacities.

A study of the structure of the constituents used in the plates, before and after formation, was made by Hughel and Hammer (8). Using a miniature negative plate, Hattorie et al. examined the same small area before and after cycling, using the scanning electron microscope and an ingenious positioning device (9). Pierson et al. showed that the surface of the negative plate differed in structure from the interior

portions (10). A structure quite different from that usually observed was reported by Weininger (11) for a polymer-bonded negative electrode. Changes in electrode structure caused by the use of lignin derivatives have also been reported (12).

The use of lignin derivatives and other organic materials as "expanders" is very important for satisfactory negative plate performance, particularly at high discharge rates and low temperatures. When no additives are present, the lead crystals obtained after formation are quite large in diameter (Figs. 6 and 7) and therefore do not react completely during discharge, because the lead sulfate product can build to a sufficient thickness on the lead crystal to prevent the remaining lead from reacting. As a consequence, the plate has low capacity and poor cycle life. The presence of lignin derivatives also retards the change from the dendritic form of lead (found in the reduced active material after formation) to the granular form (found after considerable cycling).

Therefore, commercial negative plates were used that contained lignin as well as barium sulfate; a combination demonstrated to improve capacity when high rates are used. In the investigation the plates were discharged at four different rates and examined after the 1st, 6th, 16th and 26th cycles. A scanning electron microscope and a light microscope fitted with an image analyzing system were used to detect and quantify structural changes. A Micromeritics Model 2205 high speed surface area analyzer was used to monitor changes in surface area.

Fig. 6 — Interior section broken from a negative plate that contained no expander (this piece is not plastic-impregnated). View as seen with scanning electron microscope (SEM). The plate was in the charged state after 5 cycles. Magnification 5000X.

Fig. 7 — Compare with Fig. 6. Conditions similar, except this negative plate contained 0.5% of a lignin derivative.

2. Description of Experimental Procedure

The positive and negative plates used in this investigation were commercially prepared, unformed elements. The negative plates had dimensions of 144x122x1.4 mm, not including the tab. An individual cell consisted of two positive plates and one negative plate, separated by two polyethylene separators (on each side of the negative), with 410-20 ml of electrolyte (an excess) and a Hg/Hg_2SO_4 reference electrode. The use of a single negative between two positives insured, as could be verified by monitoring the negative plate voltage via the reference electrode, that the cell reactions were constantly limited by the negative plate.

The cell potential, the potential between the reference electrode and the negative plate, and the current were continuously recorded throughout each experiment using a strip chart recorder.

The negative plates were formed in 1.200 sp. gr. H_2SO_4 at $40A/m^2$ of apparent area (both sides) for 20 hrs. At the end of the forming charge, the acid was adjusted to 1.255 sp. gr. Specific gravity at the end of charge was maintained at 1.250-1.260 during the cycling, except for one cell that was intentionally cycled in 1.190 sp. gr. H_2SO_4. A cycle series was conducted for each of 4 rates of discharge: 18, 125, 500, and 2000 A/m^2 of apparent area. This cycling extended through 26 charges, with capacity discharges after each of the first six charges, and after the 16th and 26th charge. Samples were examined after the 1st, 6th, 16th and 26th discharge. All discharges were made at room temperature (19-25°C).

Samples cut from the negative plate at each of the test points were washed in distilled water that had been boiled to remove CO_2 and O_2 and then cooled immediately before use. After 1-2 hrs of washing, the samples were dried for about 1 hr in a vacuum dessicator at 100-110°C, while being swept with a slow flow of argon. Following this, portions were examined with a scanning electron microscope, while other portions were examined as plastic impregnated sections (13) by light microscopy, using reflected light brightfield and polarized modes. An image analyzer was used to determine the relative areas of pores, lead, and lead sulfate at 500 and 1000X magnification using brightfield illumination. The BET surface area was determined using a Micromeritics Model 2205 surface area analyzer after the active material was degassed for 40 minutes at 200°C.

3. Observations and Discussion

(a) Capacity

As expected, the capacity of the negative plates slowly declined with each cycle of charge and discharge (Fig. 8). The relation between capacity and rate of discharge is also evident; the capacity decreasing with increasing rates of discharge. It will be noted that the curves have a more rapidly changing slope during the first few cycles than in later cycles. This has been observed in other experiments and is most marked under high discharge rate and low temperature conditions. We have not been able to correlate this with any single structure factor. The changes in structure dimension and surface area occurring with the first few cycles are very slight and seem

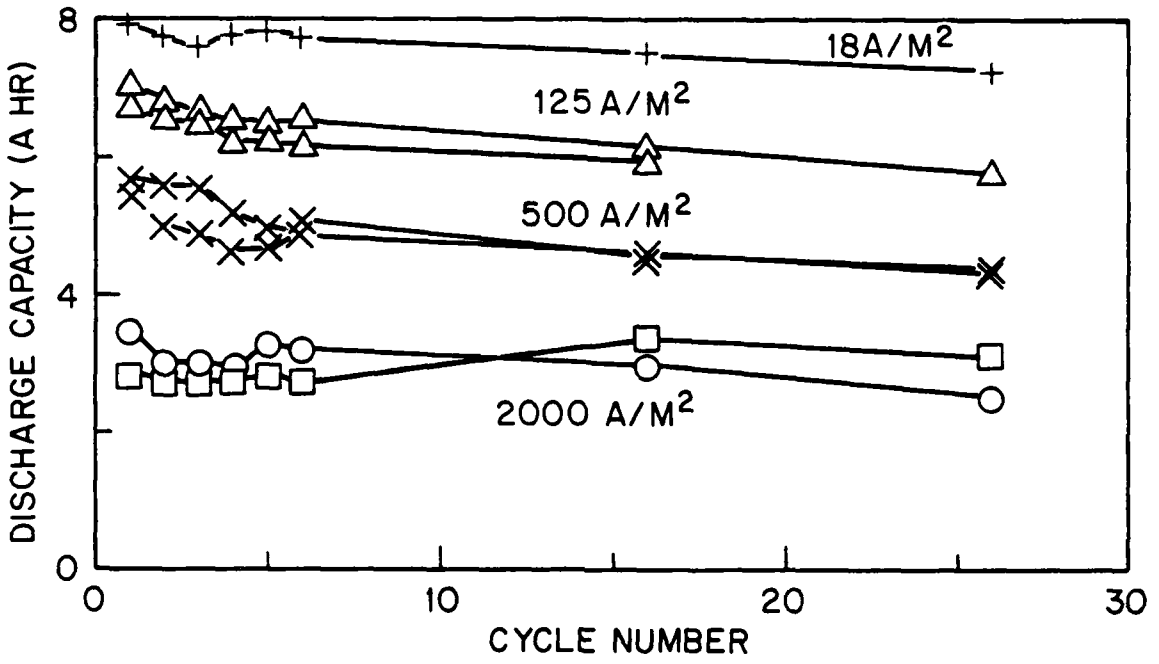

Fig. 8 — Graph showing discharge capacity obtained at different discharge rates over a period of 26 cycles, and indicating the decreasing capacity obtained with increasing rate of discharge

inadequate to explain the loss of capacity. One possible explanation is that the initial lead crystals produced in plate formation are dendritic, interconnected (Fig. 9), and conductive so that every particle is capable of entering into the first discharge process. But the first discharge changes the lead dendrites into individual lead sulfate crystals and it seems likely that when these are converted back to lead, some particles will become isolated and have limited contact with the rest of the active material, and thus fail to be converted in the next discharge. The dendritic nature of the crystals of lead clearly disappears after a few cycles, and, while the particles still appear to be interconnected, it is unlikely that they form conductive paths as good as the original uninterrupted dendrites.

Although the curves in Fig. 8 appear to have about the same slope, it is evident in Fig. 10 that higher rate discharges produce a faster loss of capacity for the same number of cycles.

Figure 10 also shows the effect of discharge rate and cycling on the negative plate potential. At the lowest rate of discharge there is practically no polarization until the end of discharge and the knee of the curve is very sharp. With increasing rates of discharge, polarization begins much earlier and the slope of the discharge curve becomes more pronounced and the knee more rounded. Note that, for each of the rates of discharge, polarization begins much earlier for the 26th cycle than for the first, with the knee correspondingly less sharp. Discharges between cycles 1 and 26 gave potentials intermediate between those shown in Fig. 10.

Fig. 9 — An illustration (SEM) of a negative plate immediately after formation, showing how the individual lead particles are extensively interconnected. The dendritic nature of this plate is more evident than in Fig. 11 because no expander is present to modify the structure. Magnification 2000X.

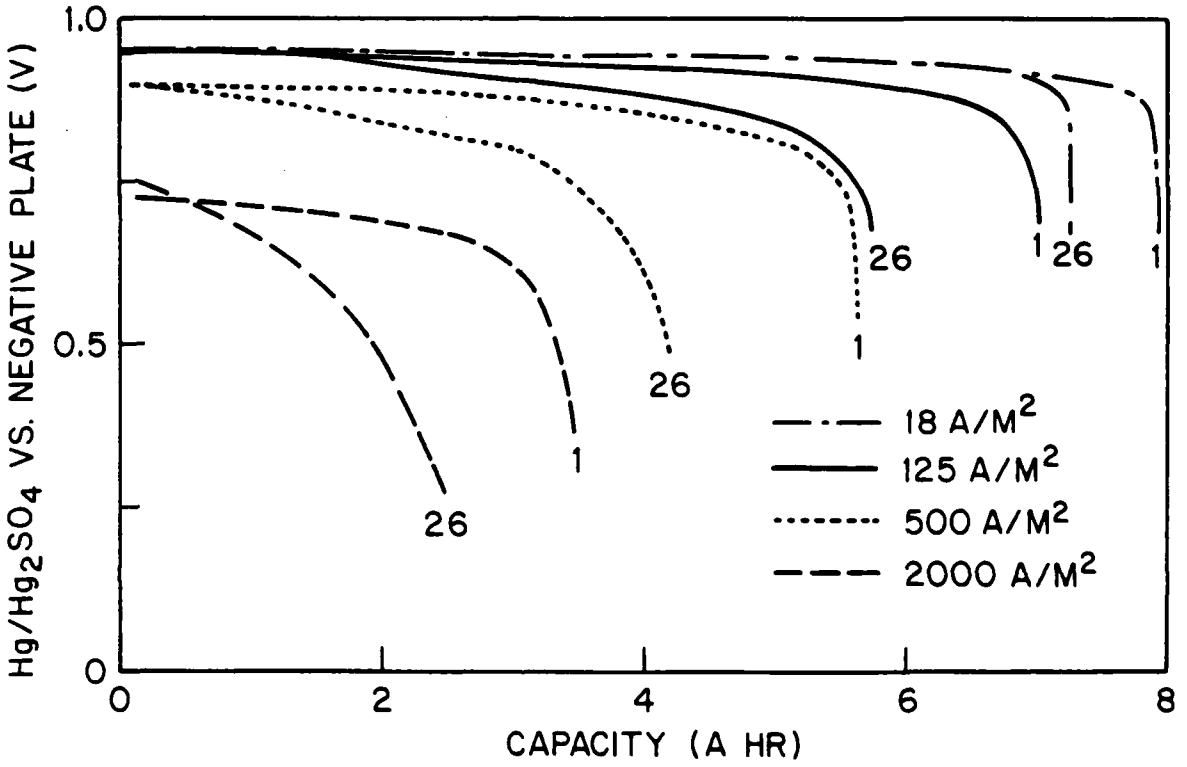

Fig. 10 — Graph showing change in polarization potential with increasing discharge rates and increasing number of cycles

(b) Structure of the discharged plate.

b1. Formed. The structure of the active material also varied with the discharge current density. The structure at the end of forming consisted of small Pb particles of 2-5 μm size. As seen by scanning electron microscopy, these particles appeared as uneven clumps of small irregular spheres (Fig. 11). These sphere-like particles were attached together in a dendritic growth but the lignin material inhibited the extension of these growthsinto recognizable dendrites of the usual pine-tree-like type. Some $PbSO_4$ crystals were still present even after forming.

Hughel and Hammer (8) showed an example of a negative plate at the end of the forming charge. In their plate the particles of lead were smoother and about half the size of those shown in Fig. 11. Because the magnifications are not exactly calibrated, no significance can be placed on the different particle size. Variations in curing and forming conditions might explain the difference in particle appearance.

b2. Discharges at $18A/m^2$ (20 hr. rate). At the end of the first cycle most of the active material consisted of $PbSO_4$ crystals of 2-7 μm in size, although some fell outside of this range. These $PbSO_4$ crystals resembled those shown in Fig. 12 but averaged about 1 μm larger. There was a slow change in the dimensions of the discharged active material with continued cycling, with more frequent appearance of larger $PbSO_4$ crystals. At cycle 26, over half of the discharged acti : material consisted of crystals in the 3-8 μm range, although many crystals

Fig. 11 — A negative plate immediately after formation where a lignin derivative was present to modify the structure. Note that magnification is higher than in Fig. 9. Magnification 5000X.

Fig. 12 — Type of $PbSO_4$ crystals at the 125 A/m^2 rate of discharge. Note the well formed rectilinear crystals. (SEM). Magnification 5000X.

had grown to 10-20 μm and a few were only 0.5-2 μm. The Pb in a charged plate was never completely converted to $PbSO_4$ during discharge, with the amount of lead remaining at the end of discharge increasing with the number of cycles.

b3. Discharges at 125 A/m^2 (2.5 hr. rate). The first discharge at this rate produced $PbSO_4$ crystals about 2-5 μm in size (Fig. 12), although ranging from 1 μm to 7 μm. These $PbSO_4$ crystals often contained holes in some of their faces, and they also increased in size with increasing cycling. At cycle 26, the $PbSO_4$ crystals were up to 10-15 μm in size, although many were still present between 2-5 μm in size. The crystal structure in Fig. 12 is much like that shown by Weininger (11) for a discharged negative plate that had received 163 cycles at 60 A/m^2.

b4. Discharges at 500 A/m^2 (0.5 hr. rate). In general, a typical $PbSO_4$ particle was only half as large for plates discharged at 500 A/m^2 as at 125 A/m^2. The $PbSO_4$ crystals most often fell in the range of 0.5-3 μm for cycles 1, 6 and 16, although the amount of $PbSO_4$ with greater size increased with cycling. Many particles up to 5 μm in width were present at cycle 16.

A large number of small Pb particles remained at the end of these discharges with a size usually under 1 μm. Optical microscopy of the polished cross sections of the plates indicated that a higher proportion of Pb remained at the end of discharge than would appear from scanning electron microscopy. These small lead particles were usually surrounded by lead

sulfate but the lead remained more likely because of isolation from the circuit rather than passivation by the lead sulfate. Optical microscopy of cross sections also showed clearly, better than the SEM, how porosity increased with cycling.

b5. Discharges at 2000 A/m^2 (5 min. rate). Most $PbSO_4$ crystals in the negative active material were between 0.4 and 2 μm after the first discharge at this rate (Fig. 13). Some crystals were as small as 0.2 μm or as large as 4 μm. The crystals of $PbSO_4$ found at 2000 A/m^2 were noticeably smaller than those formed at 500 A/m^2, and much smaller than those formed at 18 or 125 A/m^2 (Fig. 12). Again, the average crystal size tended to increase as the plate cycled. Crystals in the 2-5 μm size range became common by cycle 16, although most crystals of $PbSO_4$ were still smaller than 2 μm. A large portion of the active material remained as Pb at the end of discharges made at 2000 A/m^2, as evidenced by the much lower capacity than at the other discharge rates.

(c) Structure of the charged plates.

The plates were all charged by a standardized procedure at one rate to minimize ambiguity which might result from different charging rate effects. The type of irregular Pb surface present after the forming charge was never found after the first discharge, all subsequent charges giving Pb particles smoother than those obtained in initial forming. Typical Pb particles were 1 to 3 μm in size after cycle 6 when the active material had been discharged at 18 to 500 A/m^2. These particles were quite irregular in shape, with round rather than angular

Fig. 13 — Small $PbSO_4$ crystals of nondescript shape formed at 2000 A/m^2 rate of discharge. (SEM). Magnification 5000X.

surface features, and they often contained cavities. There was no great change in the appearance of the charged active material as cycling continued, although in the case of 18 or 125 A/m^2, the size of the Pb aggregates increased to 1-4 μm at the end of charge 27 and the surface of the particles seemed even smoother (Fig. 14). The lead surfaces often contained holes of 0.2-1 μm in diameter. Although the lead did not usually have the angular shapes of the $PbSO_4$ crystals and there was no evidence of a metasomatic change, it is perhaps significant that these holes were very similar to those that appeared in the faces of the $PbSO_4$ crystals. Lead particles with angular shapes were found most often in the charged state when using 18 A/m^2 as the discharge rate, i.e., the rate that produced the largest $PbSO_4$ crystals. The electrolyte space between particles increased as the plate was cycled and the plate itself increased in thickness.

When the discharges were at 2000 A/m^2, much of the lead in charged active material took the form of irregular clumps of small, rounded particles (Fig. 15). The small size of the Pb was evidently the result of the particles being formed from small $PbSO_4$ crystals such as shown in Fig. 13. As the cycling continued, there was a tendency for aggregates to grow together into smoother formations. Scattered crystals, and in some cases large patches, of $PbSO_4$ were found among the Pb particles of the charged plates. The amount of $PbSO_4$ in the charged plate increased with the number of cycles. The size of typical $PbSO_4$ crystals remaining after the 27th charge was 5-10 μm for a plate always discharged at 125 A/m^2 and 7-15 μm for a plate

Fig. 14 — A plate at the end of charge 27 showing the effect of repeated charges on the lead structure for 125 A/m^2 discharges. Note that the lead clumps here have a more open structure, with numerous holes, and are smoother and devoid of the fine structure seen in Fig. 11. (SEM). Magnification 5000X.

Fig. 15 — Lead in a negative plate at the end of the 16th charge, when discharges were at the 2000 A/m^2 rate. From comparison of Figs. 11, 14 and 15, it is evident that rate of discharge has an effect on the structure of the lead formed on charge, even when all charges are made at the same rate. (SEM). Magnification 5000X.

always discharged at 18 A/m^2. The disappearance of most of the smaller $PbSO_4$ crystals during a charge indicates these are more easily reduced to Pb than the larger crystals. It is probable that $PbSO_4$ crystals remaining at the end of a charge nucleate the first $PbSO_4$ formed during the next discharge, and thus grow in size before additional crystals are nucleated. In this manner such crystals would continue to grow with each discharge, and could only be destroyed by a long overcharge.

(d) Effect of acid concentration on structure.

All tests reported to this point used H_2SO_4 with a specific gravity of 1.260. Since there was an excess of H_2SO_4 in all of the cells, the acid concentration did not decrease to the extent it would in a multiplate commercial cell where the plates are tightly packed and there is little excess acid. If acid concentration has an effect on morphology, then our results could differ greatly from what happens in a commercial cell.

To guard against this possibility, a negative group was cycled in 1.190 sp. gr. H_2SO_4, using 2000 A/m^2 as the discharge current. This would be approximately the acid specific gravity of a half-discharged SLI battery. When the results using 1.190 sp. gr. acid were compared to the results for 1.260 sp.gr. acid, there was no significant difference in the appearance or size of the $PbSO_4$ crystals at the end of the discharge, nor of Pb at the end of charge. These results indicate it is unlikely that variations in electrolyte acidity would cause service batteries to have a microstructure significantly different from that found in these experimental cells.

(e) Variation of surface area with current density.

The surface area of negative plates is too low to give high reproducibility with the Micromeritics surface area analyzer. The results that were obtained are given in Table IV. Most of the values given are the average of four measurements. Five to nine measurements were made for a few of the samples having high variation. At least 16 measurements were made before reporting a value below 0.1 m^2/g. Since measurement accuracy decreased as surface area decreased, values below 0.1 m^2/g should only be regarded as an indication that the surface area was low. The results given in the upper half of Table IV show that surface area of discharged negative active material increased as the discharge current increased. This agrees with the microscopic observation that the average crystal size of $PbSO_4$ decreased as the current density increased (Figs. 12 and 13). No significant change in surface area was detected, however, after repeated cycling at any of the rates.

The unformed negative active material had a surface area of 0.82 m^2/g, which dropped to 0.23 m^2/g at the end of the forming charge. Although the four discharge rates produced different surface areas, these differences were somewhat obscured by the time the next charge was completed, since all were recharged at the same current density.

In the case of discharges at 18 or 125 A/m^2, the low surface area produced in discharge seemed to carry over and result in a low surface area for the recharged plate (Table IV). The charged sample, taken at cycle 16, for the 125 A/m^2 discharge

Table IV

BET Specific Surface Areas of the Negative Active Material, given in m^2/g

Condition	Discharge Rate (A/m^2)	Cycle 1	Cycle 6	Cycle 16	Cycle 26
Discharged	18	0.02	0.11	0.03	0.00
Discharged	125	0.16	0.14	0.18	0.17
Discharged	500	0.18	0.20	0.20	-
Discharged	2000	0.25	0.24	0.26	-
Charged	18	-	0.11	0.19	0.13
Charged	125	-	0.18	0.39	0.16
Charged	500	-	0.21	0.21	0.21
Charged	2000	-	0.21	0.19	0.20

series, was not believed to be representative. The value of 0.39 A/m^2 was unacceptably large as compared to all other samples of charged plates. This sample may have been contaminated by material from the positive plate, which has a much higher surface area, or unformed material may have been present. None of the subsequent recharges produced a surface area as high as that obtained in the forming charge. This agrees with the microscopic observation that a recharged plate contained smoother Pb particles than were obtained in a forming charge.

(f) Change in porosity.

As the negative plates were cycled, an increasing number of large voids appeared in the active material and the plates gradually expanded. At cycle 27, the plates were about 30 to 50 percent thicker than the original size. As the active material softens during cycling, it gradually becomes easier for large pores to be formed in the active material by hydrogen bubbles generated during charging (12). Expansion of the negative plates would have been more limited if the plates had been constrained, by tight packing, as occurs in cells, and fewer large voids would have been formed.

An image analyzer was used to determine porosity of the negative active material. The values given in Table V are averages of 15 to 25 measurements made at 500X magnification in steps of about 0.085 mm from one surface of the plate to the other. Areas were avoided that included the large voids. No noticeable change in porosity as a function of depth into the plate was detected. The increasing of porosity with cycles shown in Table V is at

Table V

Porosity of Negative Active Material
(percent)

Condition	Cycle	Discharge rate (A/m^2)			
		18	125	500	2000
Charged	1	-	43	48	-
Charged	6	48	48	52	52
Charged	16	49	55	54	56
Charged	26	51	52	56	57
Discharged	1	24	31	37	43
Discharged	6	35	39	46	44
Discharged	16	44	48	54	49
Discharged	26	52	-	-	-

least partially a reflection of the plate expansion, i.e., less active material per unit volume, that occurs with cycling.

Although the two plates that were examined at the end of the forming charges (Table V, cycle 1) had been treated similarly, the active material of one gave 43% and the other 48% porosity. The difference between porosity values in the different plates may therefore be in part due to differences in the original plates instead of being entirely an effect of discharge current density.

(g) Change in active material composition.

The image analyzer was also used to measure the relative amounts of $PbSO_4$ and Pb occurring in the active material. It should be stressed that the percentages reported are based on the microscopic relative areas in cross section and do not take into consideration density differences between the two materials. All measurements were at 500X except for the 2000 A/m^2 discharges, where 1000X was used because of the large number of small particles. It was found that the relative amounts of the two materials varied widely in different parts of the plate and could be different by several percent even in adjacent fields of view. The values shown in Fig. 16 are consequently averages of 15 to 35 measurements, made in a continuous series from one side of the plate to the other.

Another problem was that the shades of gray for Pb, $PbSO_4$, and void space were not widely separated, and it was difficult to set measurement thresholds on the image analyzer which would insure that all of one phase, and none of the others, was being

measured. Despite this difficulty, the trends in Fig. 16 are believed to be significant, since the same threshold settings were used for each series of samples and hence all results should be biased in the same direction.

The amount of $PbSO_4$ formed during discharge decreased as current density increased (Fig. 16), which agrees with the capacity measurements (Fig. 8). Figure 16 also shows that the amount of $PbSO_4$ present in the discharged plate slowly decreased with cycling. The opposite effect occurred in charged plates. At the end of the forming charge (cycle 1), the active material was almost 100% Pb. Samples of active material examined after cycle 26 charge contained up to 10% $PbSO_4$. These changes in charged and discharged negative plates that occur as a result of cycling are probably caused, at least in part, by gradual worsening of contact within the active material, so that some crystals become isolated either as $PbSO_4$ or as Pb.

Although random areas of high or low $PbSO_4$ concentration were common in the discharged active material, there was no significant difference between the average $PbSO_4$ concentration occurring near the surface or at the center of the plate for discharges of 18-500 A/m^2. This agrees with the results of Panesar and Portscher, who reported an even distribution of $PbSO_4$ after discharges at 15-300 A/m^2, for plates approximately the same thickness as those in the present work (14).

Measurements made at the end of cycle 1 and 6 discharges at 2000 A/m^2 indicated that the $PbSO_4$ concentration was usually a little higher near the plate surface than at the center. Figure

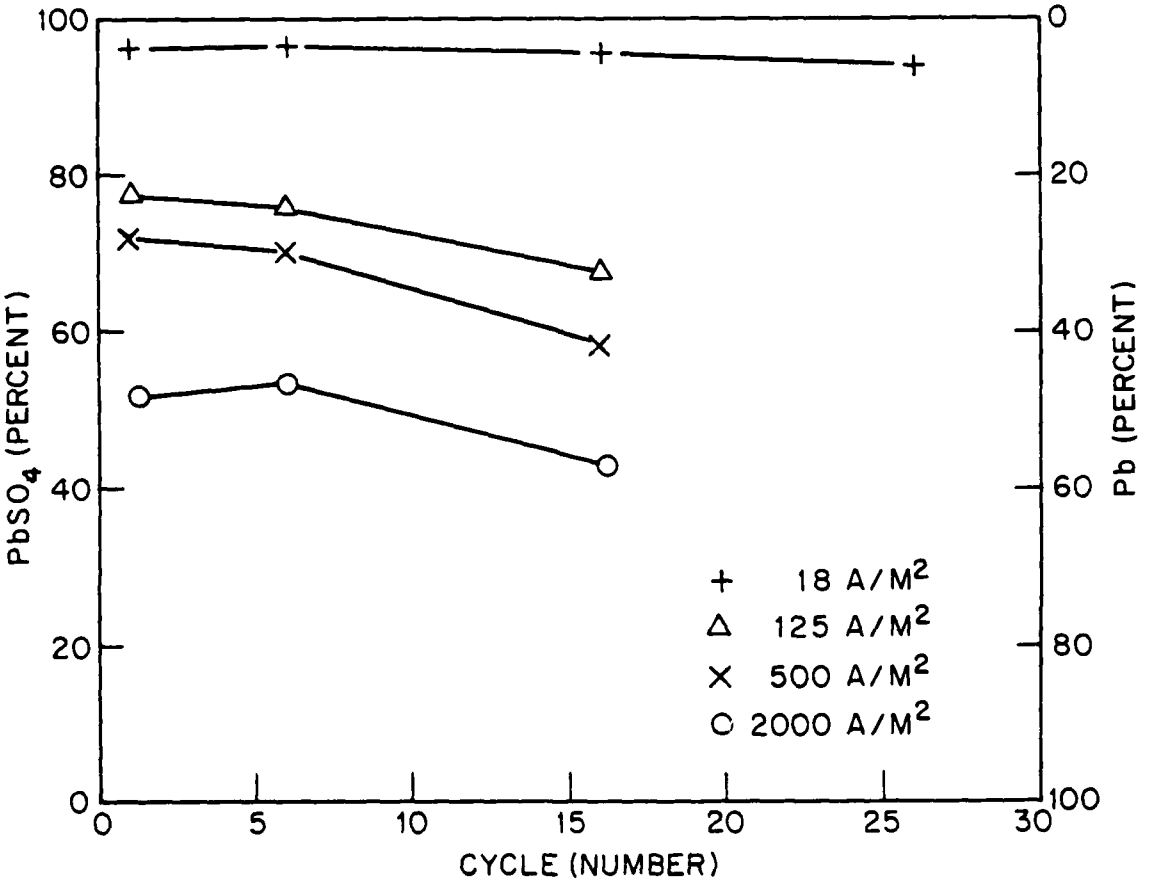

Fig. 16 — Graph showing the relative amounts of lead sulfate formed at the different rates of discharge, and with increasing cycling, as determined with the iamge analyzer

17 shows the smoothed results of 28-35 consecutive measurements extending from one plate surface to the other surface. A rapid discharge does not allow time for additional H_2SO_4 to diffuse into the plate interior after depletion of the acid originally present. As the plate gradually expands with cycling, however, more acid is available in the interior channels and there is less of an H_2SO_4 gradient. Measurements made at cycle 16, therefore, show a random distribution of $PbSO_4$ with little difference between plate surface and center.

Panesar and Portscher measured $PbSO_4$ distribution at 1800 A/m^2 (14). They found the center of the plate to have only about 50% as much $PbSO_4$ as the surface areas, a much greater difference than shown in Fig. 17. The $PbSO_4$ distribution is probably greatly affected by the type of expander employed, and by other variance in manufacture.

4. Summary

In summation, we have shown that the microstructure is changed by varying the current density, and that the effect is cumulative with continued cycling. The rates as indicated by the polarization data in Fig. 10 are, except at higher cycles, essentially diffusion-controlled across the range of discharge current. The Pb particles developed layers of $PbSO_4$ during discharge and, since the $PbSO_4$ crystals became smaller at the higher rates concurrent with a decrease in capacity, they may have formed more continuous surface layers, or "passivation" layers, which limited discharge to some extent at the higher rates of discharge. The crystal morphology indicated a solution-

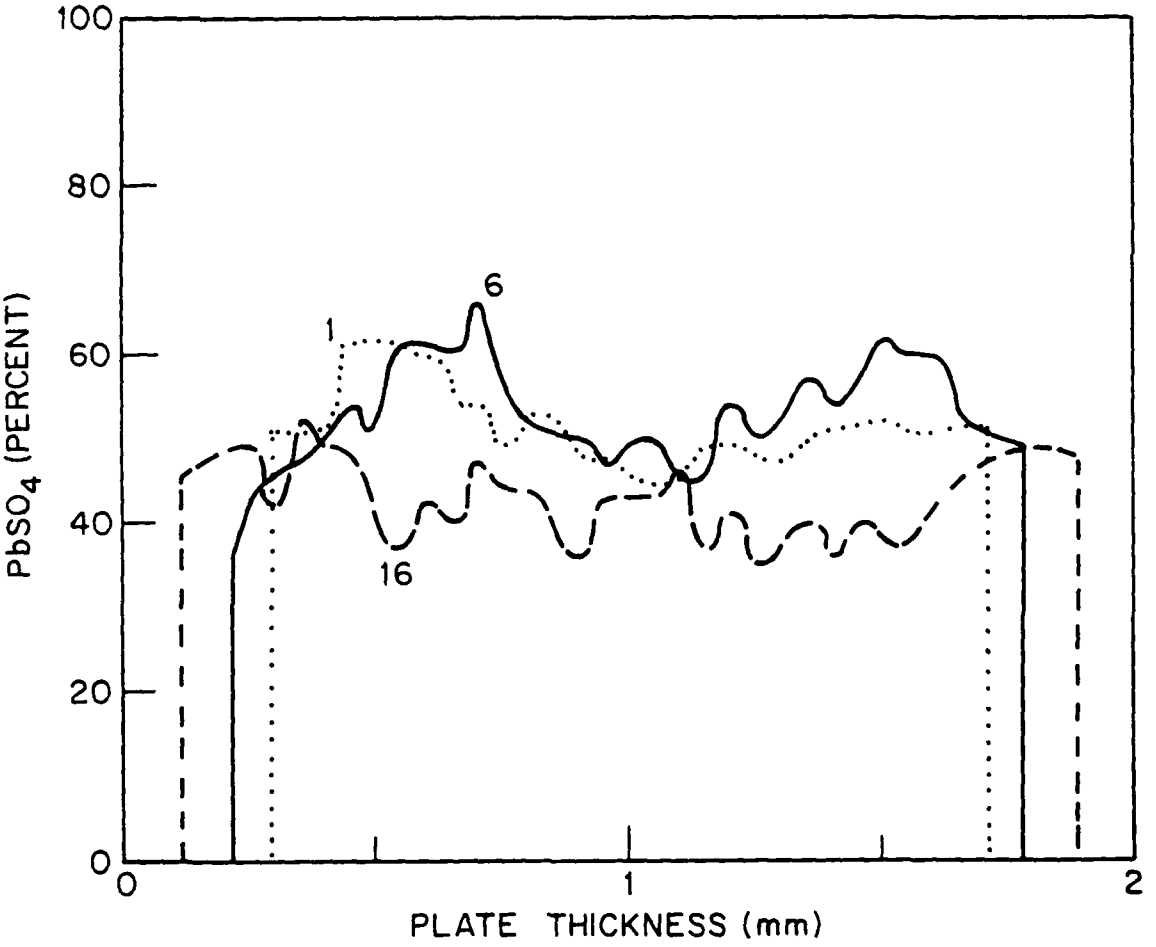

Fig. 17 — Graphic presentation of varied lead sulfate distributions across the plate section, for the 2000 A/m^2 discharge rate, at the end of cycle 1, 6 and 16 discharge. As determined with the image analyzer.

migration-precipitation process of crystal growth at all current densities, with no evidence of a solid state Pb-$PbSO_4$ reaction. The crystals of $PbSO_4$ tended to be larger the lower the current density, and at each current density, became larger with continued cycling. The changed polarizations between the first and 26th cycles in Fig. 10 are probably the result of increased resistance within the electrode mass due to lessened contact between the crystals caused by expansion of the active material, $PbSO_4$ formation, or changing crystal size and habit. It was also evident that the effects of discharge carried over through recharge and became more pronounced with each additional cycle.

It is surprising that the differences were not greater over the range of current densities studied. This would seem to indicate that the negative plate, at least, is not greatly affected by very large changes in current density. There was nc mixing of high and low rate discharges in the present experiments because our objective was to investigate the effect of repeated high rate discharges. However, alternate high-low discharge rates are also relevant to EV operation, and there is a need to know how the battery performance would be affected under these conditions. If the total capacity loss at high current density is due to diffusion-limited processes, then a subsequent discharge at low current density should give almost the original capacity. But if changes in crystal size and other effects of high current density also contribute to the capacity loss, then the next subsequent discharge at lower current density should be accompanied by considerable loss in capacity. High-low rate

discharge should be investigated to answer this question.

D. DISCHARGE RATE EFFECTS ON THE POSITIVE PLATE

1. Background

Formed positive plates may have various structures depending on paste composition, treatment, and forming conditions. Despite the initial differences, plates cycled the same way are converted to practically the same microstructure after cycling, with the structure being a function of current density and mode of operation (15). Current density has a large effect on positive electrodes of lead-acid batteries because the rate at which reactions take place is governed by diffusion and crystallization processes, with the reaction mainly involving dissolved Pb^{++} ions rather than solid state reactions (16). Other important factors that affect structure are the temperature and the proportions of α-PbO_2 and β-PbO_2 in the plate (17,18).

Discharges begin with nucleation of $PbSO_4$ on PbO_2 surfaces that are in contact with the electrolyte. Further $PbSO_4$ growth results as nearby PbO_2 is dissolved (discharged) and the Pb^{++} ions deposited as $PbSO_4$ on the nucleated $PbSO_4$ crystals (19). Eventually a continuous film of $PbSO_4$ tends to form on the PbO_2 particle surface, isolating it from the electrolyte and greatly reducing the discharge reaction. Particles of PbO_2 that remain within the $PbSO_4$ at the end of a discharge form a conductive network and serve as nuclei for crystallization of the PbO_2 during charge (2,19).

2. Experimental Procedure

The positive and negative plates used in this study were commercial plates of the type used in automotive batteries. The active materials had not been formed. Positive plate size was 144x122x1.75 mm, not including the tabs. The grids were 4% antimony-lead. Before putting a positive plate in use, active material pellets were removed to expose the grids that outlined seven equal areas on the plate. One of these seven areas was then cut from the wet plate when a sample was to be taken. Approximately 61.6 g of unformed active material remained, which was 64% of the amount originally present in a plate.

The experimental cells contained one positive plate treated as described above, two negative plates, a polyethylene separator between each negative and the positive plate, and a Hg/Hg_2SO_4 reference electrode. There was no pressure on the plates. Sheet plastic was placed parallel to the plates, filling most of the empty space inside the cell case. Removal of the plastic allowed easy withdrawal and replacement of the positive plate.

The cells contained 410-420 ml of electrolyte. The forming charge began within 30 seconds after a positive plate was put into 1.150 sp.gr. acid. A positive plate was formed 18 hours at 50 A/m^2 followed by 22.5 hours at 20 A/m^2. Then the acid was adjusted to 1.255 sp.gr. and maintained at 1.250-1.260 during the cycling. The two negative plates in a cell had a much greater capacity than the one positive plate and were formed separately.

Positive plates were discharged at 18, 125, 500 or 2000 A/m^2 geometric area. This resulted in discharges lasting, respectively, 24 hr, 3 hr, 0.5 hr, and 4 min during the first six cycles. Final cell potentials were 1.8, 1.75, 1.5 and 1.0 V. A particular positive plate was always discharged at the same current density for its entire life. Adjustments to cell current were made after removal of each sample, so that positive plate current density remained constant. Capacity discharges were done at cycles 1-6 and every ten cycles thereafter. In all other cycles, the positive plates were discharged to 80% of the previous capacity discharge. Cycling was done at room temperature (19-25°C). Charges were always done at 31.25 A/m^2, except for the forming charge.

Samples cut from the positive plates were washed 45-60 min in distilled water and then dried at 60°C. Fractured cross sections of the active material were examined using an AMR model 1000 scanning electron microscope. Other plate portions were impregnated with plastic, cut into cross sections, polished, and examined by optical microscopy. The BET surface area was determined with a Micromeritics Model 2205 surface area analyzer, using 5 g of active material broken into pieces that were 5 mm or smaller. The material was degassed 40 min at 100°C in argon before analysis.

3. Results and Discussion

(a) Capacity

Figure 18 shows the change in discharge capacity with cycling. Values for the first 26 cycles are averages of

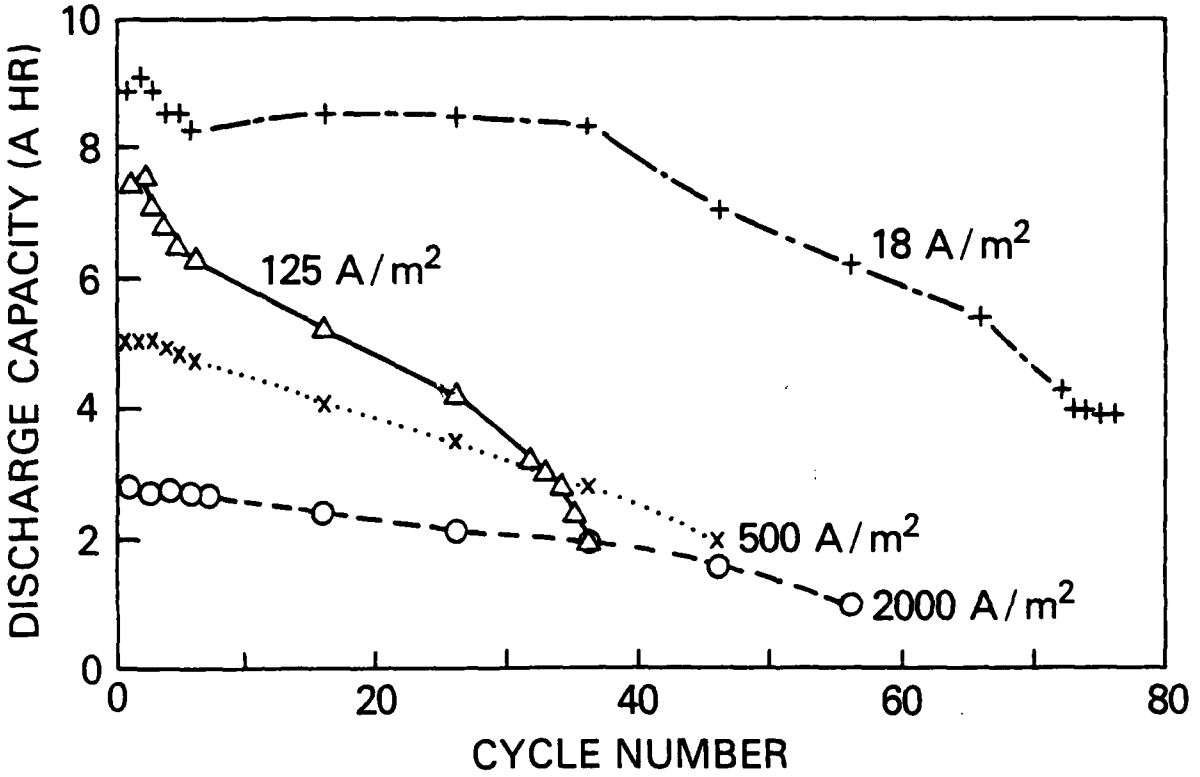

Fig. 18 — Capacity discharges of positive plates. Discharge current densities are given on the curve.

results from two or three positive plates that were cycled independently. Individual measurements deviated by an average of 2.3% from the values in Fig. 18. Values given for cycles 32 to 76 are individual measurements. When capacity declined rapidly as a plate approached failure, the discharge potential sometimes reached the cut-off value, and a plate would be 100% discharged before the next regularly scheduled capacity discharge. Capacities are compensated for the removal of samples and are given as if the quantity of active material used at cycle 1 had remained constant. Capacity and structure changed more rapidly with the deep discharges used in the present work than they would have changed if SAE cycles had been used.

During the early cycles, the capacity varied inversely with current density, as one would expect (Fig. 18). All three positive plates cycled at 125 A/m^2 showed a much greater rate of capacity loss than did the plates cycled at the other current densities. Plates discharged at 18 A/m^2 maintained their capacity much longer than plates discharged at 125-2000 A/m^2. The difference between the capacity obtained at cycles 30 to 50 when using 125-2000 A/m^2 and the capacity when using 18 A/m^2 suggests that a change in discharge mechanism occurred between 18 and 125 A/m^2.

Figure 19 gives capacities as a percent of the capacity obtained at cycle 1. If part of the active material becomes inactive after a certain number of cycles, then capacity would be expected to decrease more rapidly when cells were cycled at the lower current densities because a larger proportion of the

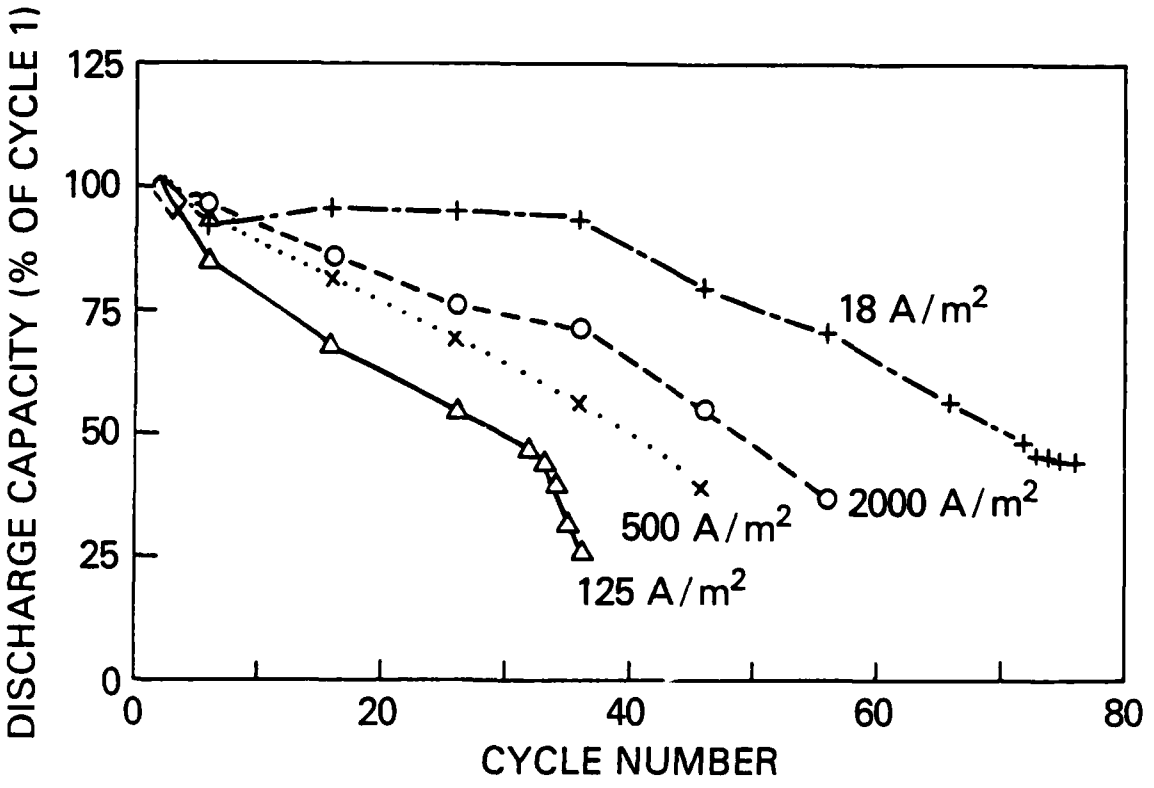

Fig. 19 — Positive plate capacity relative to the capacity at cycle 1. For clarity, the individual values at cycles 1-5 are omitted.

active material is reduced as current density is decreased. In agreement with this, Fig. 19 shows that the rate of capacity loss did increase as discharge current density decreased from 2000 to 125 A/m^2. At 18 A/m^2, however, the trend is reversed and the capacity loss is significantly lower. This suggests strongly that the discharge is limited by a different mechanism at 18 A/m^2 than at 125-2000 A/m^2. At the lowest current density used in this work, the reaction apparently had sufficient time so that diffusion processes did not limit cell capacity.

The rate of capacity loss was 0.3% per cycle for discharges at 18 A/m^2. This is the same as the rate of loss when negative plates (cf. Fig. 8) were cycled at 18 A/m^2 (20). The positive plates lost capacity at about 1.7, 1.2 and 0.9% per cycle when discharged at 125, 500 and 2000 A/m^2 (Fig. 19). These values are all higher than the 0.7% per cycle loss obtained when negative plates were cycled at 125-2000 A/m^2 (20).

The changes in positive plate potentials during discharge are shown in Fig. 20, which can be compared with potential changes in discharge for negative plates in Fig. 10. Potentials were lower in the first part of a discharge at cycle 1 and in the early cycles than they were at later cycles. The cycles between 1 and 26 gave potentials intermediate between those shown in Fig. 20. Polarization of the active material increased when current density was increased. The increased polarization was indicated in Fig. 20 by the lowered potential during the first half of a discharge, and by a decrease in the amount of discharge that was obtained before the potential began to fall rapidly.

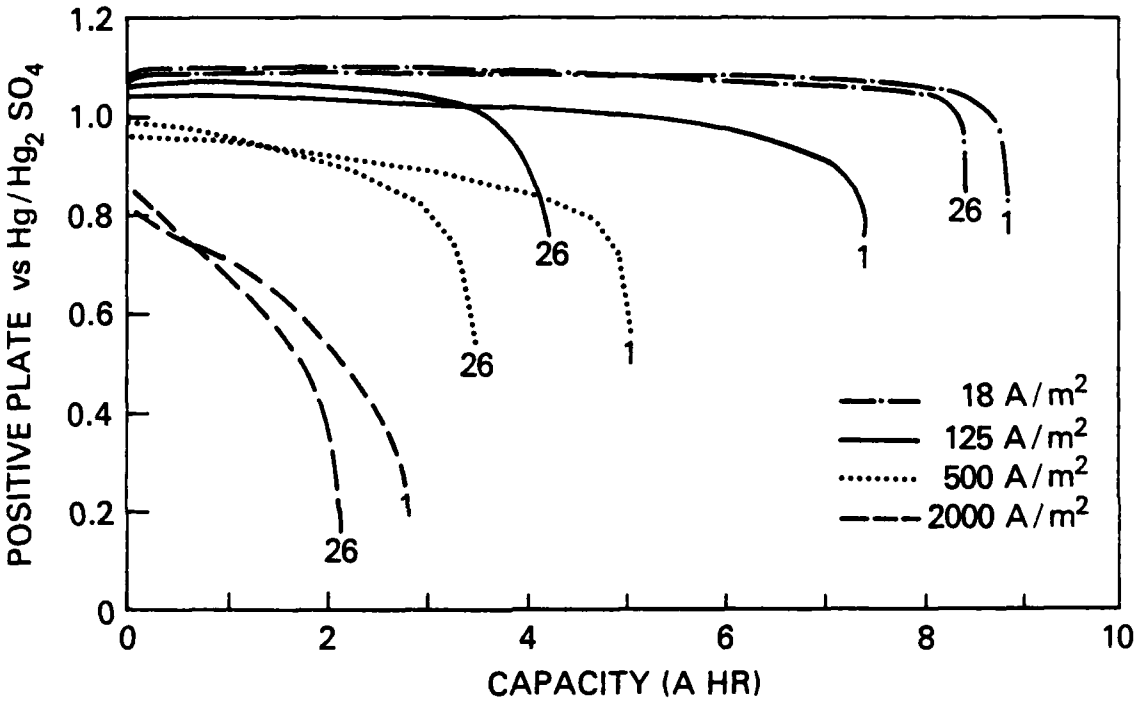

Fig. 20 — Discharge potentials between the positive plate and the Hg/Hg_2SO_4 reference electrode. Potentials are shown for cycles 1 and 26 at four rates of discharge. The current density used at cycle 1 was repeated in all subsequent discharges.

Since the negative plates in the experimental cell had considerably more capacity than the positive plates, the negative plates only varied a few hundredths of a volt during the course of a discharge. Therefore, approximate cell potentials can be obtained by adding 0.96 V, 0.96 V, 0.95 V, and 0.89 V, respectively, to the values shown in Fig. 20 for discharges at 18, 125, 500 and 2000 A/m^2.

(b) Structure of discharged positive plates

The effect of discharge current density on $PbSO_4$ crystal size was immediately evident after a single discharge of the positive plates. Scanning electron microscope photographs of fractured cross sections after discharges are shown in Figs. 21-26. The $PbSO_4$ size varied inversely with current density. The major changes in $PbSO_4$ crystal size with cycling are summarized in Table VI for the first 26 cycles. The size ranges were based on measurements of SEM photographs. To help minimize sampling error, the photographs were usually taken from at least three different samples of each electrode, and from two electrodes that were independently given the same cycling treatment. Although most of the active material was in the range of sizes given in Table VI, one could also find particles outside these ranges.

The average size of the $PbSO_4$ gradually decreased with cycling, particularly in the early cycles (Table VI). When using the lower discharge rates of 18 and 125 A/m^2, the size decrease occurred over a longer number of cycles. Samples taken later than cycle 26 from positive plates discharged at 125-2000 A/m^2

Fig. 21 — Positive active material at the end of cycle 1 discharge at 18 A/m^2, the 24-hr rate. The smallest particles are PbO_2. Medium size and large crystals are $PbSO_4$. Magnification 5000X.

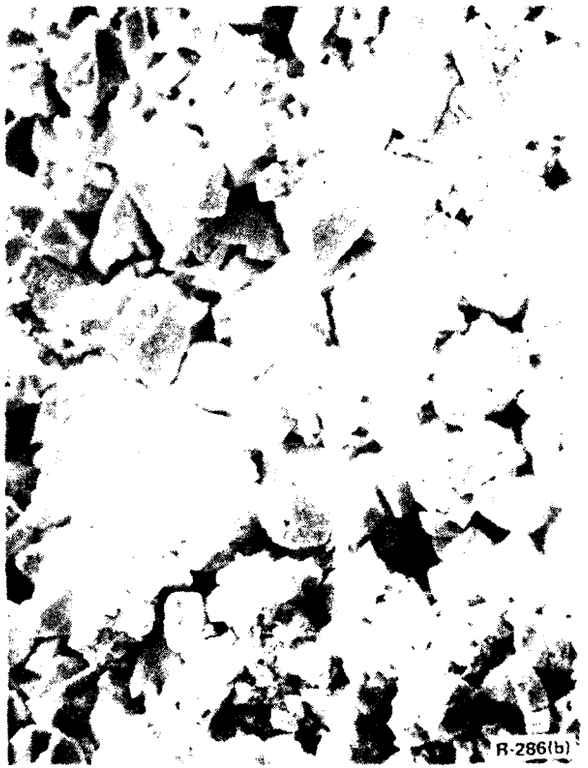

Fig. 22 — Lower magnification view of an electrode at the end of cycle 1 discharge at 18 A/m^2. Magnification 1000X. Compare with Fig. 21.

Fig. 23 — Positive active material at the end of cycle 1 discharge at 2000 A/m^2, the 4-min rate. Magnification 5000X. Note the smaller $PbSO_4$ size and increased amount of PbO_2 compared to Fig. 21.

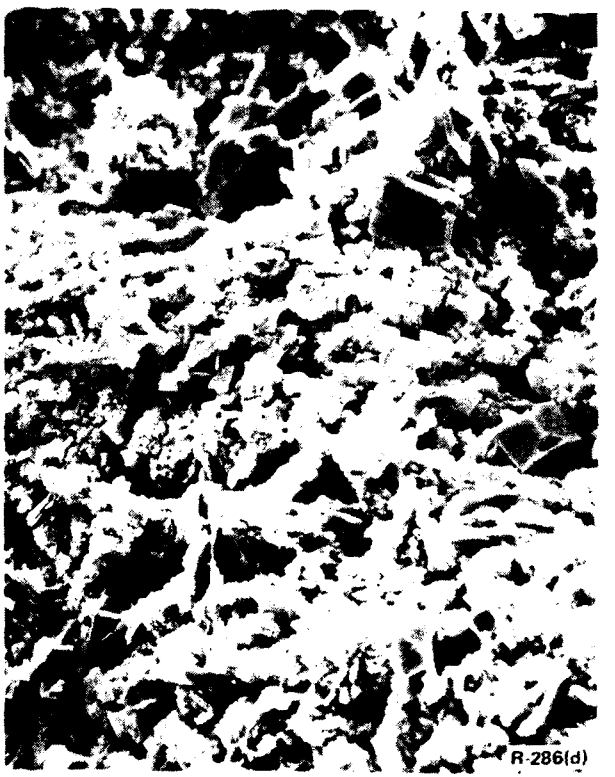

Fig. 24 — Lower magnification view of an electrode at the end of cycle 1 discharge at 2000 A/m^2. Magnification 1000X. Compare with Figs. 22 and 23.

Fig. 25 — Active material at the end of cycle 26 discharge at 28 A/m^2. Magnification 5000X. Compare with Fig. 21.

Fig. 26 — Active material at the end of cycle 26 discharge at 2000 A/m^2. Magnification 5000X. Compare with Fig. 23.

Table VI

Range of sizes that were common for $PbSO_4$ crystals in discharged positive plates
(μm)

	Current density (A/m^2)			
Cycle	18	125	500	2000
1	most 10-20 many 1-10	most 2-6 some 1-10	most 0.5-3 some 3-8	most 0.5-3 some 3-8
6	most 5-10 some 1-20	most 1-5 some 5-10	most 0.5-3 some 3-5	most 0.5-3 some 3-5
16	most 5-10 few over 10	same as cycle 6	most 0.5-3 few 3-5	same as cycle 6
26	most 5-10 sca. ce over 10	most 1-5 some 5-8	same as cycle 16	same as cycle 6

contained the same size $PbSO_4$ as was found at cycle 26 (Table VI). However, at 18 A/m^2, average $PbSO_4$ size slowly decreased for about another 20 cycles although remaining in the 5-10 μm range.

Some PbO_2 always remained in the discharged plates, and can be seen readily in Figs. 21, 23, 25 and 26. The amount of PbO_2 remaining at the end of a discharge increased as discharge current density increased (compare Fig. 21 to Fig. 23 and Fig. 25 to Fig. 26). The increased PbO_2 reflects the lower discharge capacity obtained at the higher currents. The amount of PbO_2 in discharged electrodes also increased as the number of cycles increased. At the end of cycle 6 discharge at 125-2000 A/m^2, most of the $PbSO_4$ was obscured by a PbO_2 covering. As the cycling continued, fewer and fewer $PbSO_4$ crystals were visible at the end of a discharge because of the increasing presence of PbO_2 (compare Fig. 21 to Fig. 25 and Fig. 23 to Fig. 26). Much less PbO_2 was present after discharges at 18 A/m^2 than after discharges at 125-2000 A/m^2, and here the amount of PbO_2 increased more slowly with cycling.

The examination of electrode cross sections by optical microscopy was a very useful supplement to the examination by the scanning electron microscope. The cross sections revealed some things not evident from the SEM, and confirmed others. The first discharge of the positive plates produced closely packed $PbSO_4$ (Fig. 27). The $PbSO_4$ crystals often contained PbO_2, with the amount of PbO_2 within the $PbSO_4$ increasing as discharge current increased. The SEM examinations gave no hint of the large amount of PbO_2 inside the $PbSO_4$ crystals. These PbO_2 particles play an

important part in the recharge process (2,19). As the cycling was continued, the active material gradually changed its consistency (Fig. 28).

During discharges at 18 and 125 A/m^2, the PbO_2 was reduced to $PbSO_4$ at sites throughout the electrode. Although electrodes discharged at 125 A/m^2 had the same structure at the outer layers as in the interior at cycle 1, there was a tendency for large particles to form in the interior of the electrode as the cycling at 125 A/m^2 continued. Electrodes discharged at 18 A/m^2 did not develop a difference between the outer layers and the interior. When using discharges at 500 or 2000 A/m^2, the $PbSO_4$ formed mainly near the surfaces of the electrode with some areas in the interior showing no reduction of PbO_2. Bode et al. gave similar results for the effect of discharge current density on $PbSO_4$ content (21). The areas shown in Fig. 27 and 28 were in the outer 30% of the plate, the regions where most of the reduction and oxidation took place when discharges were done at 500 A/m^2. Diffusion became an increasingly limiting factor at the higher current densities. The amount of PbO_2 remaining in the center of a discharged plate was largest when using 2000 A/m^2. Even after 56 cycles using 2000 A/m^2 as the discharge rate, some of the central areas still had PbO_2 apparently unchanged since the forming charge.

Under all of the discharge conditions, the amount of PbO_2 that remained at the end of a discharge gradually increased as the cycling continued. Increasingly large areas developed where the active material consisted entirely of PbO_2 at the end of a

Fig. 27 — Cross section through part of the positive plate at the end of cycle 1 discharge at 500 A/m^2, the 0.5-hr rate. Lightest color is PbO_2, medium gray is $PbSO_4$, and darkest gray is void space between the active material particles. Magnification 1000X.

Fig. 28 — Cross section through part of the negative plate at the end of cycle 26 discharge at 500 A/m^2. Compare with Fig. 27.

discharge. For example, after cycle 26 discharge at 125 A/m^2, an estimated 30-40% of the active material remained in the form of areas of PbO_2 without $PbSO_4$. Even at the low discharge current density of 18 A/m^2, about 15-25% of the active material consisted of separate PbO_2 areas at the end of cycle 26 discharge. After cycle 1 discharge at 18 or 125 A/m^2, no large areas consisting only of PbO_2 were found, although much PbO_2 remained within the $PbSO_4$ crystals.

At the higher discharge current densities, the development of increasing amounts of inactive PbO_2 in the electrode outer layers was partly offset by a gradual attack on the PbO_2 in the interior, the PbO_2 which had taken little part in discharges at the early cycles. As a result, the amount of PbO_2 in the interior that took little part in the discharge reaction gradually decreased with cycling. This active material in the interior must have prevented capacity from falling as rapidly as would have taken place if all of the active material had been used at cycle 1.

The amount of void space in discharged active material increased as discharge current density increased. At any given current density, the amount of voids also increased with cycling. The increase in porosity that occurred in 26 cycles can be seen by comparing Fig. 28 with Fig. 27. Since PbO_2 occupies a smaller volume than $PbSO_4$, the increased amount of PbO_2 caused the increase in void space in discharged electrodes.

The decrease in discharge capacity with cycling appeared to result from failure of PbO_2 to reduce to $PbSO_4$, rather than from

$PbSO_4$ not oxidizing on charge. Increasingly large amounts of PbO_2 remained at the end of a discharge as capacity decreased, while the amount of $PbSO_4$ in a charged electrode remained low. Loss of active material from the plates was not a major factor during the first half of the cycling. Shedding of active material became a problem late in the cycle life and may have contributed to the final drop in capacity.

Typical sizes for $PbSO_4$ found in discharged positive plates approximately equalled the range of sizes found in negative plates (compare Section III, C, 3b with Table VI), when plates discharged at the same current densities were compared. The $PbSO_4$ size tended to increase when negative plates were cycled, in contrast to the decrease when positive plates were cycled. The $PbSO_4$ concentration was only a little higher near surfaces of negative plates than in the interior after discharges at 2000 A/m^2. This contrasts with the strong difference found in positive plates. The amount of charged active material remaining in the negative plates at the end of discharges increased with cycling, the same as in the positive plates. The negative plates differed also in showing an increase in the amount of discharged active material remaining at the end of charges.

(c). Structure of charged positive plates

Charged plates that were given an equal number of cycles generally resembled each other when examined by the SEM regardless of which discharge rate was used. Charged active material consisted of clumps of PbO_2 containing small PbO_2 crystals about 0.1-0.3 μm in size. Typical clump size was 1-4 μm

after cycle 6 charge. Clump size was smallest in electrodes that had been discharged at 18 A/m^2. Clump size decreased between cycle 6 and 16, and then remained approximately constant. A few of the PbO_2 clumps contained small $PbSO_4$ crystals.

When cross sections of charged positive plates were viewed by optical microscopy, very little $PbSO_4$ was found. The charged plates that had always been discharged at 18 A/m^2 had a uniform structure throughout the active material with PbO_2 present as small particles. Charged plates given repeated cycles with discharges at 125 A/m^2 gradually developed larger PbO_2 clumps in the interior of the plates, while the PbO_2 near the surface remained small. The PbO_2 clumps were randomly distributed at cycle 6 when using this current, but were mainly in the center of a cross section at cycle 16 and later.

Charged plates that had been discharged at 500 or 2000 A/m^2 always had large clumps in the center of the plates. These large clumps rather closely resembled the PbO_2 that was present at the end of the forming charge. It is assumed that a slight reduction of the PbO_2 in the interior had taken place during discharge. Oxidation of the small amount of $PbSO_4$ which had formed in the interior caused the slight change from the appearance at the end of the forming charge. Charged electrodes given 26 or more cycles using 2000 A/m^2 as the discharge rate had smaller particles in the interior near the grid than elsewhere in the interior, but these particles near the grid were still larger than the PbO_2 in the outer layers.

Particles in the outer layers of a charged electrode always

discharged at 500 A/m^2 resembled the small particles found when using 18 or 125 A/m^2. Particles in the outer layers were much larger at cycle 6 in charged plates always discharged at 2000 A/m^2. Here the $PbSO_4$ that developed during a discharge was on the surface of large PbO_2 clumps. The centers of the original PbO_2 clumps were not reduced in the early cycles. In later cycles, increasing amounts of small PbO_2 crystals were present in the outer layers of plates always discharged at 2000 A/m^2.

(d) Active Material Consistency

When samples were removed for examination, it was obvious that the consistency of the active material was strongly affected by cycling conditions. After cycle 1 discharge at 18 A/m^2, the active material was much harder than after cycle 1 at higher current densities. Charged active material was always a little softer than discharged active material at the same cycle. Initially, the active material was fastened firmly to the grids. Then the active material gradually softened with cycling. The active material became quite fragile by the time 50% of the original capacity was lost, and the grids became brittle.

These changes can be correlated with structural changes observed in the active material. The unusually large $PbSO_4$ crystals that formed during cycle 1 discharge at 18 A/m^2 (Table VI) gave the active material a hardness never found under other conditions. Smaller $PbSO_4$ crystals presented more opportunity for movement of the active material when a force was applied, and thus the active material was softer when smaller $PbSO_4$ predominated. The PbO_2 particles were much smaller than $PbSO_4$ and

gave the active material less strength. It has been mentioned that increasing amounts of the PbO_2 became inactive with cycling. Part of the inactivity may be caused by loss of physical contact with the conducting grids. If so, this lack of contact would contribute to the loss of strength that was observed.

(e) Surface area variations

It has been shown that the surface area of formed positive plates increased as the proportion of β-PbO_2 to α-PbO_2 increased (18,22,23). Formed positive plates in the present work averaged 5 m^2/g, which is reasonable for a mixture of α- and β-PbO_2. The BET specific surface area decreased as acid concentration decreased, being 7.5 m^2/g in 3.5 M H_2SO_4 and 5.2 m^2/g in 1.5 M H_2SO_4 for formed positive plates with high β-PbO_2 content (18). Capacity was not proportional to the surface area of formed positive plates (18).

The specific surface area of discharged positive electrodes showed a strong effect of current density (Fig. 29). The values in Fig. 29 can be compared to results of Voss and Freundlich (see Fig. 9 of reference 17), where β-PbO_2 plates would be expected to give BET specific surface areas of about 2.0, 3.0 and 5.2 m^2/g after discharges at 18, 125 and 350 A/m^2, respectively. Cycle number was not specified. Wiesener and Reinhardt reported surface areas about 3 m^2/g in the early cycles at 20°C, slowly rising to about 4.5 m^2/g at cycle 75 (23).

The large $PbSO_4$ crystals that were produced at a low current density (Fig. 21) gave a low surface area to electrodes discharged slowly. Discharged electrodes had larger surface areas

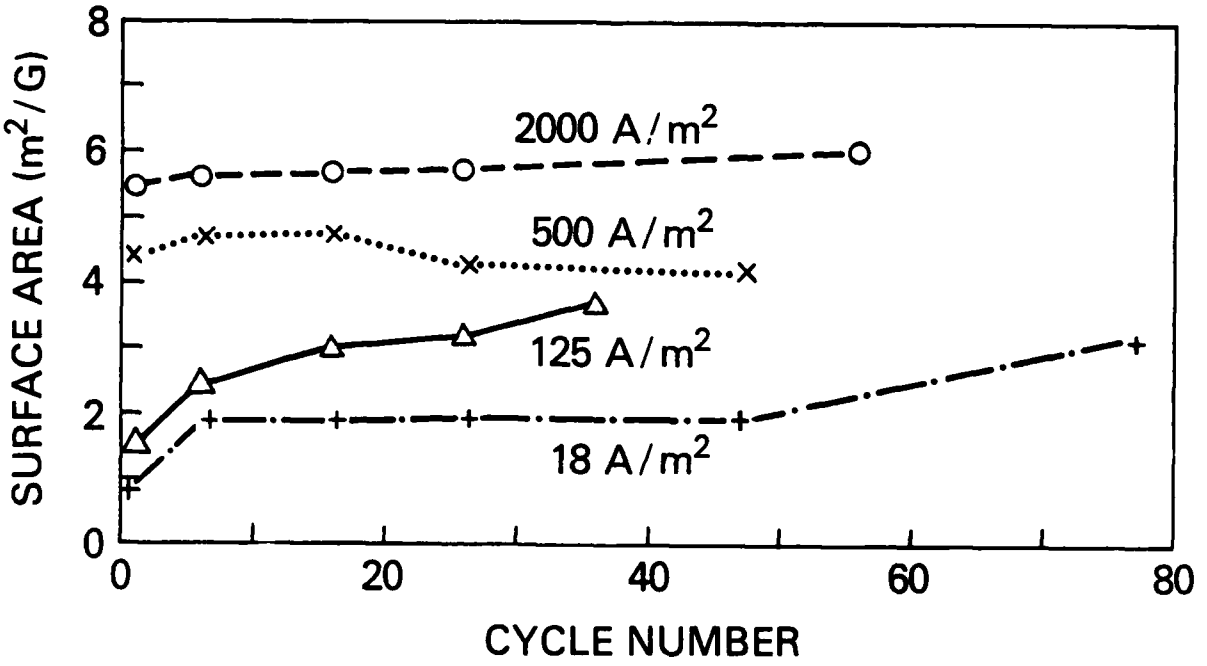

Fig. 29 — BET specific surface areas of positive active material at the end of capacity discharges

when higher current densities were used. Surface area increased because the average size of the $PbSO_4$ crystals was smaller and also because less $PbSO_4$ formed before the discharge ended, resulting in larger amounts of PbO_2 remaining in the electrode at the end of a discharge at the higher current densities.

Charged active material always had a higher surface area than discharged active material. Compare Fig. 29 with Fig. 30. A higher surface area is to be expected in charged active material because PbO_2 particles are much smaller than $PbSO_4$ crystals. One might expect all of the charged electrodes to give the same surface area, since all used the same charge current density. However, the structures produced during discharge were not entirely destroyed during charge. Electrodes with the lowest surface area after a discharge tended to have the lowest area after being recharged. The differences in the charged active material were not nearly as great as the differences in the discharged active material.

As cycling progressed, the values for charged and discharged surface areas tended to approach each other. This was caused by increasing amounts of $PbSO_4$ remaining in the charged electrode and increasing amounts of PbO_2 remaining in the discharged electrode as the capacity slowly decreased with cycling.

The specific surface area of unformed positive active material was 0.7 m^2/g, about the same as the 0.8 m^2/g for unformed negative active material (Section III,C,3e; also ref. 20). At the end of the forming charge, the specific surface area of the positive active material had increased to about 5 m^2/g, while

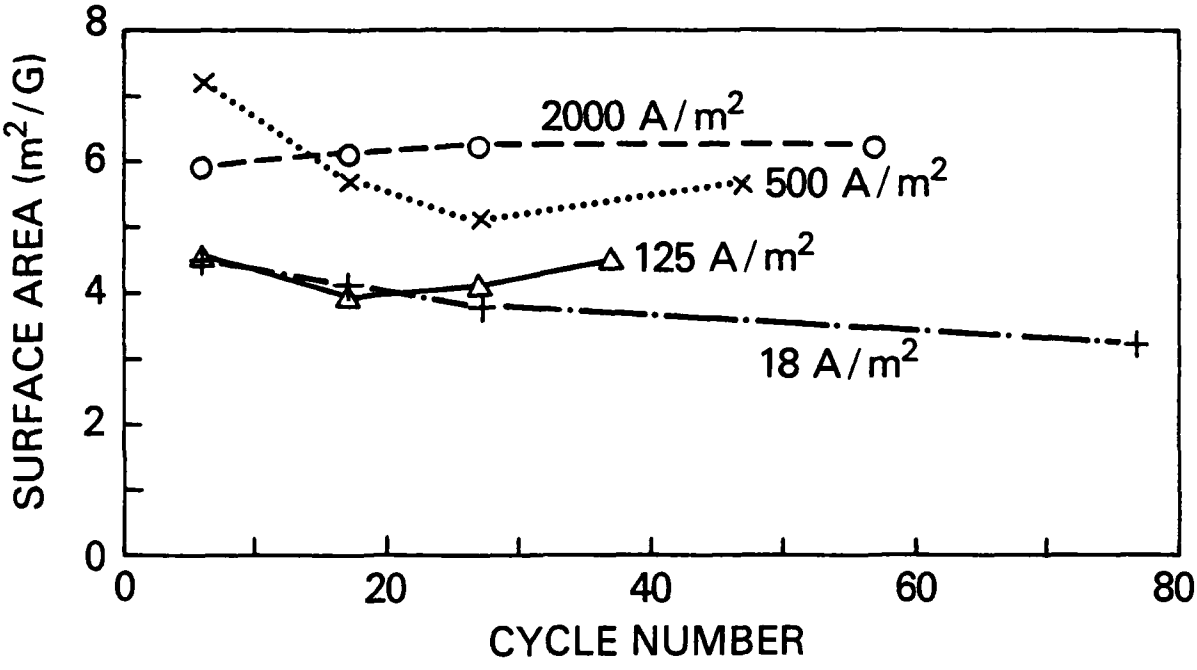

Fig. 30 — BET specific surface areas after charges at 31.25 A/m^2. These positive electrodes were always discharged at the current densities given on this figure.

the negative active material had decreased to only 0.2 m^2/g. Throughout the cycling, the charged negative active material had only 3-4% of the surface areas given in Fig. 30, and discharged negative plates had only 4-6% of the values given in Fig. 29. This difference was caused by the high surface area of the PbO_2 particles always present in positive plates and the low surface area of the Pb particles in negative plates. It is surprising that discharged plates had such a great difference in surface area, since the sizes of $PbSO_4$ in positive and negative plates were relatively close to each other. Obviously the PbO_2 and Pb that remained in the discharged plates had a strong effect on specific surface area.

4. Summary and Conclusions

Positive plate capacity decreased with cycling because of PbO_2 failing to be reduced during discharge, instead of $PbSO_4$ not being oxidized during charge. An increasing proportion of the active material became inactive as the electrodes were cycled. The rates of capacity loss were 0.9, 1.2, 1.7, and 0.3%, respectively, for discharges at 2000, 500, 125 and 18 A/m^2. There were several indications that the reaction at 18 A/m^2 was limited by a different mechanism than the diffusion processes which limit discharges at the higher rates.

The active material consistency was strongly affected by cycling conditions. The hardest active material was obtained after the initial discharge at 18 A/m^2, and was caused by the unusually large $PbSO_4$ crystals that developed. At all discharge current densities, the active material gradually softened with

cycling as smaller crystals developed. The active material became quite fragile by the time that half of the original capacity was lost, and the grids became increasingly brittle.

The $PbSO_4$ crystal size varied inversely with current density and gradually decreased with cycling, particularly in the early cycles. The $PbSO_4$ crystals often contained PbO_2 that was not evident until the $PbSO_4$ crystals were cut open. In addition, as the cycling continued, large areas of PbO_2 remained in discharged electrodes. The amount of void space in discharged electrodes increased with cycling and when discharge current density increased.

Further work should be done to determine the reasons for the apparent change in mechanism when low discharge rates are used. Work should also be done to determine why part of the PbO_2 becomes inactive with repeated cycling. The inactivity may result partly from a change in the PbO_2 structure, and partly from loss of electrical contact.

IV. STUDY OF CORALLOID STRUCTURE IN CYCLED POSITIVE PLATES

A. BACKGROUND

The effect of varied rates of discharge on both negative and positive active material has been described in the foregoing sections.

In addition to the changes in the positive material that can be directly related to rate of discharge or charge, other changes occur that are directly related to the number of charge and discharge cycles and only indirectly affected by the rate. For

example, following formation, the positive active material possesses a compact and uniform structure with very small and evenly distributed voids (Fig. 31,32). As cycling continues, the structure changes, so that much larger voids are formed and the active material between them is compacted into a continuous network. The structure is reminiscent of brain coral, so we have used the term coralloid for its description. Figure 33 is an SEM micrograph of the structure. Cross sections examined by optical microscopy show the compact nature of the PbO_2 network between the voids (Fig. 34).

Because of the irregular nature of the coralloid structure and because it is sometimes overlaid with loosened particles, it is not as easy to detect by SEM as with cross sections prepared for optical microscopy.

The coralloid structure was first thought to be beneficial, since the dense network of PbO_2 appeared to offer strength and good conductivity to the active material, and the apparently interconnected voids to allow ready access of electrolyte to all parts of the structure. However, more extensive investigation has failed to confirm that the coralloid structure is beneficial. Instead, the development of the coralloid structure has been found to be accompanied by reduced capacity. It is probable that the large amount of PbO_2 made inaccessible by the dense packing within the PbO_2 network is a direct cause of this reduced capacity. Permeability studies have also shown that there is practically no flow of electrolyte through the structure, indicating that the voids are not continuously connected as they appear.

Fig. 31 -- A broken section of formed positive plate (no plastic impregnation). Note very small particles and small voids or pores. (SEM). Magnification 1000X.

Fig. 32 — A plastic impregnated metallurgical cross section of formed active material. Dark areas are voids, light areas PbO_2 particles. Both Figs. 31 and 32 demonstrate the small pores and relatively dense packed lead dioxide structure found in a formed but uncycled plate. (Optical microscope). Magnification 800X.

Fig. 33 — The coralloid structure which develops in the positive plate with cycling. Compare with Fig. 31 which shows the positive plate following formation. (SEM). Magnification 1000X.

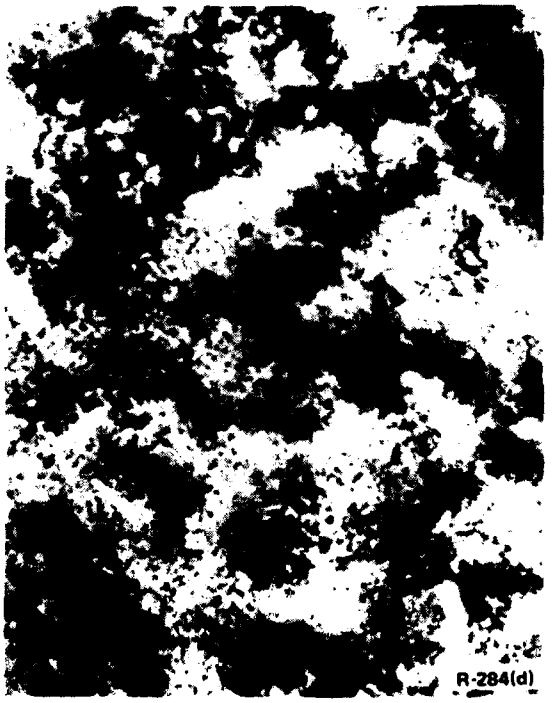

Fig. 34 — The coralloid structure seen in cross section by light microscopy. The light areas are PbO_2, the dark areas are voids in the coralloid mass. Magnification 1000X.

B. OBJECTIVES

Our research objective has been shifted therefore from efforts to promote coralloid structure to attempts to prevent its formation. This has proven to be impossible up to this point. Some of our earliest work had shown that every pasted plate studied (15), regardless of manufacture or point of origin, converted to the coralloid structure when cycled. However, it seemed possible that tubular plates, because their method of manufacture is so different from pasted plates, might not show this tendency to produce coralloid structure. For pasted plates, lead oxide is mixed with water and H_2SO_4 and pasted into the grids as a mixture of PbO, $PbSO_4$, and various basic lead sulfates. The grids are then given a long cure (drying) to homogenize and stabilize the structure before forming. In tubular plate manufacture, the dry lead oxide is simply placed in tubular containers and, after a brief soaking period, formed directly.

C. EXPERIMENTATION

To investigate the possibility that tubular plates might not form the coralloid structure, tubular plates were prepared from three different oxides, two proprietary and the third a mixture of a proprietary oxide with red lead. These plates were soaked for various lengths of time before forming: 1 min., 15 min., and 15 hrs. at 20°C, and 15 hrs. at 75°C. However, for each of these plates, the coralloid structure began to form after ten charge-discharge cycles, and was well defined throughout the active material by 100 cycles (Figs. 35 and 36).

Fig. 35 — Coralloid structure found in tubular plates after 100 cycles. (SEM). Magnification 1000X.

Fig. 36 — Cross section of coralloid structure in tubular plate after 100 cycles. Note the dense, thick branches of the coralloid structure and the lack of porosity within the branch structure. (Optical microscope.) Magnification 1000X.

Another plate with an unusual method of preparation is employed in the Bell telephone cylindrical cell. This plate is prepared with pure tetrabasic lead sulfate which is mixed with water to form a thick paste and then pressed into the plate, dried, and formed (24). Formation of this plate produces an active material with an unusual structure which we have designated as reticulate. As formation takes place, a continuous film of PbO_2 is formed on the surface of each tetrabasic lead sulfate crystal. The appearance and composition of this film is different than the interior of the crystal. This film becomes continuous at points where the crystals contact one another and forms a cell-like network throughout the active material that acts as a microgrid (Fig. 37). Work at this laboratory (25) had shown that this microgrid is extremely durable, and acts to prevent active material softening in batteries with lead-calcium grids when these batteries are maintained at a float potential. It seemed possible that such a microgrid might restrict the formation of the coralloid structure in batteries that were cycled.

Therefore plates were made from pure tetrabasic lead sulfate and water, and from a PbO-H_2SO_4-H_2O mix that was converted to tetrabasic lead sulfate by heat and high humidity, and cycle-tested. But in both cases, the reticulate network only lasted 10-15 cycles before the coralloid structure became evident.

A third type of unconventional plate was also tested. In earlier NRL studies on flow-through electrodes, a method had been developed to produce positive plates with a pseudo-

Fig. 37 — Reticulate structure in a formed plate, resulting from the use of tetrabasic lead sulfate as the original paste. This cross section shows the manner in which a hard, dense shell of PbO_2 (lightest-appearing material) forms around each tetrabasic lead sulfate crystal and, in the aggregate, produces a continuous cell-like structure throughout the formed active material. (Optical microscope.) Magnification 500X.

Fig. 38 — Lead dioxide pseudo-dendritic structure yielding a porous positive plate. This is a cross section where the light areas are PbO_2 and the darker areas represent porosity. Magnification 800X.

dendritic structure of very porous nature (Fig. 38). This excessive porosity was thought possibly to be a means of at least slowing coralloid formation, but it was found once again that the active material soon converted to the coralloid structure with cycling.

D. CONCLUSIONS

It is thus more certain now than ever that the coralloid structure is essentially a product of cycling, and that its occurrence is independent of the type of oxide or method of plate preparation.

It is still possible that the coralloid structure could be modified for better performance, and this avenue is being explored, but as yet with little success. The coralloid nodes are so thick that much of the PbO_2 in their interior remains unreacted, either because of the very low porosity of the nodes themselves (Fig. 34), or because they allow formation of $PbSO_4$ layers thick enough to passivate the remaining PbO_2 core (Fig. 39). A solution would be to reduce the node diameter, or perhaps increase its porosity. The last might not be effective, however, since we know that the coralloid structure ultimately becomes porous with extended cycling (Fig. 40) but with a loss, rather than increase, in capacity.

Altering the node diameter appears more promising, and we have demonstrated that the coralloid dimensions are affected by the presence of antimony (smaller node diameters) and calcium (larger node diameters). Unfortunately, however, the effect is

Fig. 39 — Coralloid structure in a discharged plate. Lead sulfate crystals have formed a dense layer over the surface of the lead dioxide structure originally present. While a portion of the lead dioxide has been dissolved in the formation of the lead sulfate, sufficient lead dioxide remains so that the coralloid nature of the original structure is plainly outlined by the lead sulfate crystals that cover it. (SEM). Magnification 1000X.

Fig. 40 — A cross section showing the breakup of coralloid structure after prolonged cycling (284 cycles). The formerly thick coralloid branches have mostly disintegrated into a much less dense and more porous mass, although some of the large pores associated with the coralloid structure still remain. (Optical microscope.) Magnification 800X.

small with the amounts of Sb and Ca that can be used without inducing deleterious effects in other parts of the battery, and the node diameter is not decreased enough to be expected to significantly increase capacity. The necessity that the additive must withstand the rigorous conditions within the plates (e.g., organic additives would be quickly oxidized and lost at the positive plate), and have no harmful effects in any other aspect, greatly limits the candidates. And, although many materials have been considered and a number used as additives in the paste, none so far has been more than marginally successful in reducing the coralloid dimensions without at the same time producing effects that shorten battery life.

Another possibility that we have recently begun to consider is that the repeated growth and escape of gas bubbles during gas generation in the final stage of charging could both compact the active material and open channels to the surface so as to produce the coralloid structure. Plans are being made to test this theory by cycling within voltage limits that would preclude gas generation. The cause of the coralloid structure, and the factors which influence it, has thus remained elusive, but since the coralloid formation represents one of the fundamental reactions of electrode active material and appears to be linked with the capacity and life of the battery, we believe the effort has merit and should be continued.

V. TUBULAR POSITIVE PLATE STUDY

A. INTRODUCTION

Tubular positive plates have already been mentioned in con-

nection with coralloid structure, but there are other important reasons for studying this type of plate more carefully.

First, tubular plates are more adaptable to assembly-line production than flat pasted plates and require fewer energy-consuming steps and less storage facility. The mixing of the heavy paste requires considerable power in itself, and there is the complexity of pasting the grids, which must be followed by slow and careful drying (carried out in specially maintained rooms) to homogenize the active material and prevent excessive shrinkage and cracking.

The tubular plate, on the other hand, requires no preliminary mixing of the oxide, unless a blend of oxides is used. Even in that case, the mixing involves dry powders and requires much less energy than wet mixing. Pasting is avoided, since the dry powder is simply poured into the tubes (which are vibrated for even packing) to fill the space around the central spline which serves for current collection. The tubes are then capped, given a brief acid soak (mainly to prevent oxide dust from sifting through the pores of the tube material), dried rapidly (without the precautions required for pasted plates), and formed.

The second, and often most important, advantage of tubular plates is that they can give a much longer life than pasted plates, although with less ability to deliver high rate discharges.

B. OBJECTIVES

A search of the literature shows that while considerable study has been made of the behavior of pasted plates, there is

hardly any mention of tubular plates. We have become interested in the tubular plate for several reasons. Batteries with tubular positive plates have been suggested for use in vehicle propulsion and for this reason alone should be studied to learn more about the effect of this type of operation on internal factors such as crystal morphology and grid corrosion. Because tubular plates have a long life and can be cycled hundreds of times, the changes that occur in the growth and decay of the coralloid structure take place more slowly and offer a better opportunity for study than with pasted plates. This is also true for other morphological changes that occur during cycle life.

Since the principal disadvantage of the tubular plate is its inability to deliver high discharge rates and since high discharge rates are required in EV use, we have undertaken a study of tubular plates at various stages of cycling, in the prospect that this would suggest means for increasing the discharge current density. The success of tubular positive plates also suggests that it may be possible to produce an active material of equal or better quality than obtained in flat plates, while bypassing the state-of-the-art formulations and uncertainties involved in paste mixing and pasted plate curing.

For the investigation of the tubular positive plate, we obtained unformed positives from several manufacturers that had been made with several different oxides and blends. We also arranged to obtain plates that had been cycled for various lengths of time. Although this investigation has been limited,

several generalizations can be made that are believed to hold true in all cases.

C. RESULTS AND CONCLUSIONS

1. Effects of Soaking

From information supplied by manufacturers, there appears to be little agreement as to the necessary period of soaking, or its effects. As mentioned previously, plates in our investigation were soaked for 1 min., 5 min., 15 min., and 15 hrs. at 20°C, and for 15 hrs. at 75°C. It was found that there was hardly any greater penetration of the acid after 15 minutes than after 1 minute (Figs. 41 and 42). Even after 15 hrs., the acid had not wetted the powder entirely, except in the case of the 75°C soak (Figs. 43 and 44). It was evident that the dilute sulfuric acid penetrates far enough in one minute to insure that a film of lead sulfate is formed sufficient to prevent loss of the fine PbO powder in subsequent handling.

When the acid first penetrates the powder, it forms $PbSO_4$, which passivates the surfaces of the PbO particles encountered. The increased volume of the lead sulfate also blocks the pores so that additional penetration proceeds very slowly. With increasing penetration, the acid becomes increasingly neutralized so that instead of normal lead sulfate, $PbSO_4$, basic lead sulfates and hydroxides are formed. This produces a whole series of crystal shapes, some of which are represented by Figs. 45, 46 and 47. These photographs are part of a series taken to show the changes in crystal form that occur from the outer edge of the powder to the limit of acid penetration. We have not yet

Fig. 41 — A cross section through a tubular plate. The tube can be seen as a thin dark line around the edge. The dark area within the tube, with the very irregular inner boundary, shows the extent of the sulfuric acid penetration after one minute of soak. The lighter zone within this circle is untouched powder. The dark circle at the center is the spline that extends through the tube as a current collector. The tube was impregnated with plastic before sectioning, and the apparently open cracks are actually filled with the plastic. Magnification 8X.

Fig. 42 — Conditions similar to Fig. 41 except with a 15-min acid soak. There is little, if any, greater penetration than for the one-minute soak. The projections from the central spline are tabs to insure that the spline remains centrally located in the tube. Despite these tabs, the spline here seems to have been displaced somewhat from a central position. Magnification 8X.

Fig. 43 — This section illustrates that even 15 hrs of soaking at 25°C does not give acid penetration entirely to the center, as a small circle of unchanged dry oxide remains around the central core. Magnification 8X.

Fig. 44 — This section shows complete penetration occurred when the acid was held at 75°C for 15 hrs. Magnification 8X.

AD-A111 453 NAVAL RESEARCH LAB WASHINGTON DC F/G 10/3
RESEARCH ON LEAD ACID BATTERY ELECTRODES.(U)
FEB 82 A C SIMON, S M CAULDER, C P WALES EC-76-A-31-1003
UNCLASSIFIED NRL-MR-4751 NL

END
DATE FILMED
3-82
DTIC

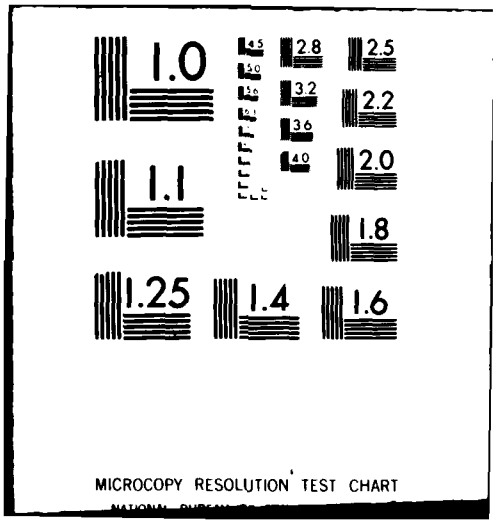
1.0
1.1
1.25
1.4
1.6
1.8
2.0
2.2
2.5
2.8
3.2
3.6
4.0
MICROCOPY RESOLUTION TEST CHART

Fig. 45 — This shows the type of crystals that occurred next to the tube, where the acid first penetrated. Figures 46 and 47 show illustrations of the type of crystal structure found where the acid had penetrated to a greater depth. These are only a few of the types of crystals noted along the acid concentration gradient, and they have not yet been identified. (SEM). Magnification 5000X.

Fig. 46 — See Fig. 45

Fig. 47 — See Fig. 45

identified each of these crystal types, but it seems that they have no effect on the structure found in the plate after forming.

There was no significant difference in the structure of the formed plate, nor in its subsequent performance or length of life, regardless of the length of soak. There thus appears to be no value in an acid pre-soak before formation except as a means of preventing loss of powder during fabrication.

It is evident that as the acid penetrates, it passivates the PbO and forms lead sulfate that blocks the pores and prevents further penetration except at extremely slow rates. When electrolytic formation begins, the different normal and basic lead compounds at the outermost surface will be converted to the more open and porous PbO_2, allowing additional surface acid to penetrate. The additional acid will convert the basic compounds to normal lead sulfate, which in turn will form more PbO_2. This process is repeated many times, with the acid gradually penetrating throughout the entire powder as it is converted to PbO_2.

2. Coralloid Structure

While the use of different oxides caused some differences in the structure of the formed plates made from them, these differences had disappeared by 100 cycles and only the usual coralloid structure was seen. Although no difference could be detected in the structures from different oxides after cycling, the performance and life did seem to depend to some extent on the oxide used.

3. Bursting of Tubes

After about 1200 cycles, the tubes began to show evidence of bursting. It is commonly believed that bursting results from too much oxide being introduced into the tubes initially. In other words, too much vibration tends to compact the powder and increase density so that when lead sulfate (of greater volume) is formed in subsequent cycling, internal pressure is generated that is sufficient to break the tube. While this may possibly occur in some cells, it was not found to be the cause here. In all examinations, it was found that the excess volume that caused bursting was generated by corrosion of the spline and its conversion to lead dioxide. Whereas the volume change in the conversion from PbO_2 to $PbSO_4$ is a more or less constant factor, remaining the same with each discharge, the progressive corrosion of the spline, where Pb is converted to PbO_2, produces a constantly increasing volume change (Figs. 44 and 48).

At the end of 1200 cycles, the active material still showed evidence of coralloid structure except at the outer portions of the tube where the active material had developed a structure that seemed to consist entirely of isolated and separate particles when viewed in cross section (Fig. 49). That these particles were not separate and isolated from one another, however, is indicated by several facts. In the first place, we have repeatedly observed that the inflow of the slightly viscous plastic used for impregnation will carry loose particles before it and concentrate them at the interior of the structure

Fig. 48 — Cross section of a tubular plate after over 1200 cycles. The small, light-appearing, irregular patch at the center of the tube is all that remains of the metal spline (compare with Fig. 41). This remaining metal is surrounded by a ring of dense black PbO_2 which is part of the corrosion product. Note also the featureless material that occurs in a circular zone just within the container tube, as contrasted with the active material nearer the center. This zone is discussed in the text and in the next photograph. Magnification 8X.

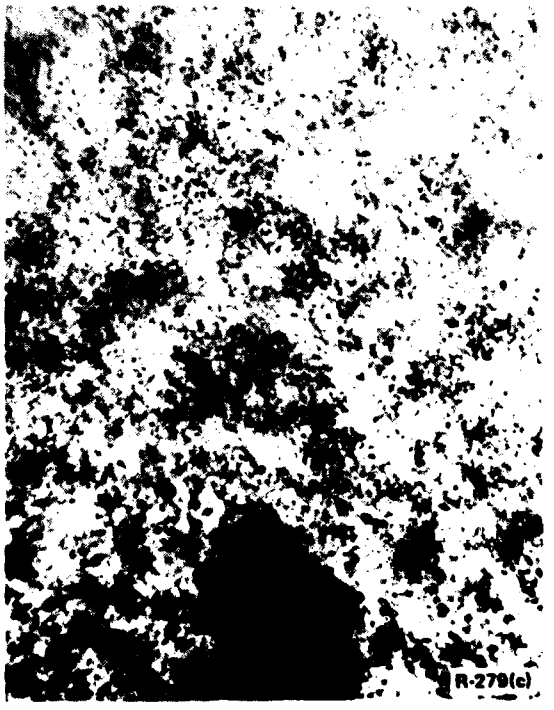

Fig. 49 — A view at higher magnification of the featureless zone referred to in Fig. 48. This impregnated section shows that, except for one large pore at the bottom of the photograph, the material is composed of a very fine network of PbO_2 with very small pores. There is no suggestion of a coralloid structure in this outer zone, although coralloid structure can still be found closer to the central spline. Magnification 500X.

where they are, in effect, "filtered out." No such disturbance of these particles was noticed; no particles were found to have been carried inward into the coralloid structure where they would have been easily observed.

Also, if the particles were indeed separate and unconnected, it is improbable that they could transmit sufficient pressure to cause the tube to burst. With the spaces that exist in the coralloid structure and between the particles making up this outer layer of active material, the only manner that pressure could be exerted from the growing volume of PbO_2 produced by spline corrosion is through a rigid structure. Therefore it must be assumed that both the coralloid structure and the "separated" particles in the outer zone constitute rigid bodies with connections above or below the plane of the section. This seems to be borne out by SEM examination.

A third point that indicated that the particles are attached to one another and not loose is the fact that they are found in uniform distribution from top to bottom of the tube. If they were loose, it would be expected that they would eventually shift through the structure to become concentrated in the lower portion of the tube. There is good reason to believe therefore that the particles in the unique outer layer formed after 1200 cycles in the tubular plates are connected to one another, even though the points of contact may be much more limited than in earlier structures that existed in the plate.

4. Active Material Retention

Weight measurements before cycling and after 1200 cycles indicate a weight loss of about 6-10%, so presumably some active material is lost as sediment that sifts through the porous tube. This performance, however, is much better than the active material retention normally found with the usual flat, pasted plate used in electric vehicles.

VI. CONSULTATION

In addition to research, personnel assigned to this research program have contributed significantly to the DOE battery and electric vehicle (EV) development effort through diagnosis of test EV battery failure, and review of patents, research proposals, and other literature pertaining to the lead-acid battery. Program members have also assisted DOE by providing information and perspectives to show the benefit of the lead-acid battery in DOE programs, and by appearing before DOE and Congressional Committees concerned with these matters.

REFERENCES

1. S. M. Caulder, J. S. Murday, and A. C. Simon, J. Electrochem. Soc., 120, 1515 (1973).
2. A. C. Simon, S. M. Caulder, and J. T. Stemmle, J. Electrochem. Soc., 122, 461 (1975).
3. H. M. Rietveld, J. Appl. Cryst., 2, 65 (1969).
4. R. W. C. Wyckoff, "Crystal Structures," Interscience Publishers, N.Y., p. 403, 1963.
5. A. Tolkacev, Vestnik Leningradskogo Univ., No. 4, 152 (1958).

6. J. Leciejewicz and I. Padlo, Naturwissenschaften, 44, 373 (1962).

7. W. R. Busing, K. O. Martin and H. A. Levy, ORFLS Report ORNL-TM-305. Oak Ridge National Laboratory, Tennessee, 1963.

8. T. J. Hughel and R. H. Hammer, "Power Sources 3," D. H. Collins, Ed., p. 35, Oriel Press, Newcastle-upon-Tyne, (1971).

9. S. Hattori, M. Yamaura, M. Kohno, Y. Ohtani, M. Yamane, and H. Nakashima, "Power Sources 5," D. H. Collins, Ed., p. 139, Academic Press Inc., New York (1975).

10. J. R. Pierson, P. Gurluski, A. C. Simon, and S. M. Caulder, J. Electrochem. Soc., 117, 1463 (1970).

11. J. W. Weininger, J. Electrochem. Soc., 121, 1454 (1974).

12. A. C. Simon, S. M. Caulder, P. J. Gurlusky and J. R. Pierson, J. Electrochem. Soc., 121, 463 (1974).

13. A. C. Simon and E. L. Jones, J. Electrochem. Soc., 102, 279 (1955).

14. H. S. Panesar and V. Portscher, Metalloberfl., 26, 252 (1972).

15. A. C. Simon and S. M. Caulder, J. Electrochem. Soc. 118, 659 (1971).

16. D. Berndt, "Power Sources 2," D. H. Collins, Ed., p. 17, Pergamon Press, Oxford, England (1970).

17. P. Reinhardt, M. Vogt and K. Wiesener, J. Power Sources, 1, 127 (1976).

18. E. Voss and J. Freundlich, "Batteries 1," D. H. Collins, Ed., p. 73, Pergamon Press, Oxford, England (1963).

19. A. C. Simon, C. P. Wales and S. M. Caulder, J. Electrochem. Soc., 117, 987 (1970).

20. C. P. Wales, S. M. Caulder, and A. C. Simon, J. Electrochem. Soc., 128, 236 (1981).

21. H. Bode, H. Panesar and E. Voss, Chem.-Ing.-Tech., 41, 878 (1969).

22. D. Kordes, Chem.-Ing.-Tech., 38, 638 (1966).

23. K. Wiesener and P. Reinhardt, Z. Phys. Chem., Leipzig, 256, 285 (1975).

24. R. V. Biagett and M. C. Weeks, Bell Technical J., 49, 1305 (1970).

25. A. C. Simon, "Batteries 2," D. H. Collins, Ed., p. 63, Pergamon Press, New York (1965).

26. P. A. D'Antonio and A. Santoro, Acta Cryst. B36, 2394 (1980).


DATE
ILME